REPORT DOCUMENTATION PAGE

Form Approved
OMB No. 0704-0188

AD-A206 438	**1b. RESTRICTIVE MARKINGS**

3. DISTRIBUTION / AVAILABILITY OF REPORT

Approved for public release;
distribution is unlimited.

4. PERFORMING ORGANIZATION REPORT NUMBER(S)

5. MONITORING ORGANIZATION REPORT NUMBER(S)
AFOSR-TR- 89-0436

6a. NAME OF PERFORMING ORGANIZATION	6b. OFFICE SYMBOL (If applicable)	7a. NAME OF MONITORING ORGANIZATION
University of California, Irvine. Dept. of Mech. Engr.		AFOSR/NA

6c. ADDRESS (City, State, and ZIP Code)	7b. ADDRESS (City, State, and ZIP Code)
University of California, Irvine Irvine, CA 92717	Building 410, Bolling AFB DC 20332-6448

8a. NAME OF FUNDING / SPONSORING ORGANIZATION	8b. OFFICE SYMBOL (If applicable)	9. PROCUREMENT INSTRUMENT IDENTIFICATION NUMBER
AFOSR/NA	NA	AFOSR-86-0016

8c. ADDRESS (City, State, and ZIP Code)	10. SOURCE OF FUNDING NUMBERS			
Building 410, Bolling AFB DC 20332-6448	PROGRAM ELEMENT NO. 61102 F	PROJECT NO. 2308	TASK NO A2	WORK UNIT ACCESSION NO.

11. TITLE (Include Security Classification)

(U) Fundamental Studies on Spray Combustion and Turbulent Combustion

12. PERSONAL AUTHOR(S)
Sirignano, William A. ; Samuelsen, Gary Scott

13a. TYPE OF REPORT	13b. TIME COVERED	14. DATE OF REPORT (Year, Month, Day)	15. PAGE COUNT
Annual Technical	FROM 87/11/01 TO 88/10/31	89/2/06	70

16. SUPPLEMENTARY NOTATION

17. COSATI CODES			18 SUBJECT TERMS (Continue on reverse if necessary and identify by block number)
FIELD	GROUP	SUB-GROUP	Spray Combustion, Turbulent Combustion, Atomization

19. ABSTRACT (Continue on reverse if necessary and identify by block number)

Four major research tasks were performed during the year. Several prototype liquid atomization experimental designs were developed and tested, and the pulse visualization system was demonstrated. A nonlinear theory for liquid sheet deformation has been developed that predicts vortical rollup of the liquid-gas interface and allows for a rough estimate of early ligament dimensions in the atomization process. The turbulent reactive flow study identifies that the mixing and entrainment rates are identical on the high-speed and low-speed sides of a constant-density mixing layer. The formation, merging, and pairing of vortical structures is also predicted. Variable property effects have been included in the vaporizing droplet theory providing significant modifications on drag coefficients, Nusselt number, and Sherwood numbers. Modified correlations for higher transfer numbers are being developed and interacting droplets are considered.

20. DISTRIBUTION / AVAILABILITY OF ABSTRACT	21 ABSTRACT SECURITY CLASSIFICATION
☒ UNCLASSIFIED/UNLIMITED ☒ SAME AS RPT ☐ DTIC USERS	Unclassified

22a. NAME OF RESPONSIBLE INDIVIDUAL	22b TELEPHONE (Include Area Code)	22c OFFICE SYMBOL
Julian M. Tishkoff	(202) 767-0465	AFOSR/NA

DD Form 1473, JUN 86   Previous editions are obsolete

AFOSR ANNUAL TECHNICAL REPORT

REPORTING PERIOD: 1 NOVEMBER 1987 - 31 OCTOBER 1988

FUNDAMENTAL STUDIES ON SPRAY COMBUSTION
AND TURBULENT COMBUSTION

AFOSR GRANT 860016D

PREPARED BY: W.A. SIRIGNANO, CO-PRINCIPAL INVESTIGATOR

G.S. SAMUELSEN, CO-PRINCIPAL INVESTIGATOR

R.H. RANGEL, ASSOCIATE INVESTIGATOR

C.-H. CHIANG, RESEARCH ASSISTANT

F. MIRALLES-WILHELM, RESEARCH ASSISTANT

B.E. STAPPER, RESEARCH ASSISTANT

DEPARTMENT OF MECHANICAL ENGINEERING

UNIVERSITY OF CALIFORNIA, IRVINE

SUBMITTED TO: J.M. TISHKOFF

1 FEBRUARY 1989

TABLE OF CONTENTS

I. SUMMARY

Four major research tasks were performed during the year. Several prototype liquid atomization experimental designs were developed and tested, and the pulse visualization system was demonstrated. A nonlinear theory for liquid sheet deformation has been developed that predicts vortical rollup of the liquid-gas interface and allows for a rough estimate of early ligament dimensions in the atomization process. The turbulent reactive flow study identifies that the mixing and entrainment rates are identical on the high-speed and low-speed sides of a constant-density mixing layer. The formation, merging, and pairing of vortical structures is also predicted. Variable property effects have been included in the vaporizing droplet theory providing significant modifications on drag coefficients, Nusselt number, and Sherwood numbers. Modified correlations for higher transfer numbers are being developed and interacting droplets are considered.

II. INTRODUCTION

The AFOSR Program on Fundamental Studies of Spray Combustion and Turbulent Combustion has centered on four major tasks during the reporting period from 1 November 1987 to 31 October 1988. Significant progress has occurred on each task. The major objectives and the major accomplishments are summarized later in this section. Details are provided in the next section entitled Research Status. Of course, even further information is contained in the publications listed in Section IV.

The three theoretical tasks have each yielded some very noteworthy results and collectively have resulted in ten publications and four presentations at conferences and seminars appearing in the last year ending October 31, 1988. See Sections IV

1

and V. The experimental task has resulted in a functioning apparatus that is yielding interesting results. Further publications in each of the task areas are expected. The program staff has remained reasonably stable. Professors Samuelsen and Sirignano, Drs. Rangel and Sowa, and Messrs. Chiang, Miralles-Wilhelm, Stapper, and Crum continue with the program. Dr. Raju has left for a position elsewhere. No degrees were granted during the reporting period. The professional personnel are listed in Section VI.

A summary of the objectives and major findings and accomplishments during the past year follows for each task.

A. ATOMIZATION EXPERIMENT

The goal of the experimental program is to observe and quantify the deformation of a liquid sheet between the point of injection and the point of breakup. Of specific interest are the wave length and wave amplitude of the deformed sheet. The objective of the current year has been to establish and demonstrate an experimental fixture that produces the desired condition, and to establish and demonstrate a visualization system for conducting the measurements.

During the year, a prototype test fixture (labeled Prototype II) was fabricated based on design changes implemented to reduce the pressure drop in the nozzle inlets and to improve the machinability of the fixture. The prototype was tested and found to produce a sheet of higher quality than that obtained using the Prototype I fixture. The quality of the sheet, however, was not sufficient to meet the goals of the program. Longitudinal striations in the formed sheet continued to persist although a substantial improvement was noted over Prototype I. Three scenarios have been identified to obtain the quality of sheet desired: (1) Reduce surface roughness within the nozzle, (2) increase the liquid flow velocity, and (3) improve the internal nozzle

hydrodynamics.

By the end of the current reporting period, the first scenario was addressed with favorable results. Teflon was sprayed on the internal surfaces of Prototype II, and a third experimental fixture (labeled Prototype III) was machined from INCONEL to improve material strength and resistance to corrosion, and the surfaces were machined to minimize surface roughness. Improvements in the quality of the liquid sheet were clearly evident. At the end of the reporting period, steps were initiated to address the second and third scenarios, both of which are likely contributors to the sheet quality.

The pulse visualization system was demonstrated using a non- UV-optimized imaging lens. The system will become fully operational when a custom made UV lens package arrives early in the next reporting period. With the UV lens package in place, the system will be used both in a continuous-filming and a single-shot mode, the latter of which will be used to perform the computer image enhancement routines and sizing calculations for the sprayed sheet.

B. ATOMIZATION THEORY

It is well known that the efficiency of a liquid-fueled combustor depends critically on the efficiency of the vaporization process which is strongly dependent on the droplet size distribution resulting from the atomization mechanism. Deterministic models of atomization processes are still in their infancy, even for the simplest configurations. Some empirical models based on a few more or less ad hoc assumptions exist, but the simulation of the evolution of a large liquid mass going through a nonlinear deformation process and breakup eventually resulting in a spray is still to come. Our efforts in this area are devoted to the study of the nonlinear shear distortion of a planar liquid sheet interacting with a stream of air on each side. The effect of surface tension as well as that of a density dicontinuity are included.

3

Linear theory results have been generalized to include the finite-sheet case. The critical wavenumber is shown to be weakly dependent on the sheet thickness when the density ratio is very small, as in air-liquid systems. The numerical calculations show qualitative differences as the sheet thickness decreases or as surface tension increases, mainly a disappearance of the rollup features encountered in the single-sheet case. Some dimensions of the early ligaments in the breakup process can be estimated.

C. TURBULENT REACTIVE FLOWS

The two-way interaction between the fluid dynamics and the rate of energy release plays a fundamental role in the evolution of turbulent reactive flows. The objective of this study is to gain a better understanding of the transport processes that occur in turbulent flows, particularly, the interaction and relative importance of the different rate-controlling factors. Mixing rate and reaction rate predictions for turbulent mixing layers are a further objective. Developments during the reported year have occurred along two directly related fronts. On one hand, the species concentration and probability density function distributions in an array of non-interacting viscous vortices have been obtained by an approximate analytical approach. When comparing the results with experiments reported in the literature, it is found that the lack of symmetry shown in the experiments is associated with a bias of the measurements, and not with real differences in mixing rate. Results for the mixedness parameter indicate that the mixing process is enhanced by increasing the vortical strength, and weakly influenced by molecular diffusivity.

The second approach being developed relaxes the assumption of noninteractive vortical structures by considering the evolution of the flow field from its initial configuration consisting of a surface of discontinuity to the formation and interaction of large scale vortical structures. During the phase reported here, the efforts have been concentrated on understanding the fluid mechanics that control the pairing

4

and merging process and the ways in which it can be controlled by means of appropriate external excitation. It is shown that the interaction, grouping, and eventual merger of large-scale vortical structures is the result of basically two distinct phenomena: the shearing effect of the initial layer configuration which tends to bring the structures together so that pairing can occur, and the spreading effect of viscous diffusion which is responsible for the merger of the structures.

D. VAPORIZING DROPLET CALCULATIONS

The general objective of this study is the detailed analysis of a vaporizing droplet or an interesting group of vaporizing droplets in a convective environment. In order to determine the dimensions and predict performance, stability, and pollutant emission of a combustor design, the trajectory, heating and vaporizing history of a droplet must be accurately computed. Hence this research has been focusing on the accurate investigation of the local transport processes as well as the overall parameters describing the system such as net drag force, heat and mass transfer around the droplet. It is also desirable to obtain the relationship between the transfer coefficients and some important fluid parameters such as heat, mass transfer numbers and Reynolds number.

The unsteady Navier-Stokes equations are numerically solved with minimum assumptions. The numerical calculation is performed in generalized coordinates over a computational domain, which is accordingly adjusting to the moving interface boundary. The effect of variable properties, which is believed to be very important in a typical high pressure and high temperature flow field, is the main consideration during this research. The results indicate that the constant properties case overpredicts the drag coefficient at least by 20%. The drag coefficient does not simply increase with time as a result of the reduction of Reynolds number. It is noteworthy that the transfer number plays a very important role in the droplet transport phenomena. For higher transfer numbers, the vaporization rate is larger and the drag

5

coefficient can be significantly reduced. For lower transfer numbers, the boundary layer blowing effect is weaker and the droplet acts more like as a solid sphere while the drag coefficient is dominated by the Reynolds number reduction. The correlation of Renksizbulut and Haywood does not agree with our results for the range of transfer numbers considered in the present calculation.

We have examined the interacting effects between two vaporizing droplets which are moving in tandem with respect to the free stream, in an intermediate-Reynolds-numbers-flow over a limited range of different initial Reynolds number, droplet spacing, and droplet radii ratio. A very sophisticated grid generation technique is employed to accommodate the changing boundary shapes. The basic solution procedure is the same with the single droplet case. The constant properties assumption (except gas-phase density) is used to simplify the algorithm involved solving interface boundary conditions simultaneously. The results show that the droplet interactions are evident for initial Reynolds numbers of 50 to 200 and for initial droplet spacing of 2 to 15 droplet diameters. The droplets can either collide or move apart depending upon the initial conditions. There exists a critial ratio of initial droplet diameters $a'_{2,0}/a'_{1,0}$ below which droplet collision becomes unlikely. The momentum, heat and mass transfer processes are quite different for two droplets depending upon the spacing. For a sufficient spacing, both droplets behave as two isolated droplets. When the droplet spacing becomes too small, the downstream droplet is fully covered by the wake of the lead droplet and the heat transfer is significantly reduced.

III. RESEARCH STATUS

A. ATOMIZATION EXPERIMENT

Experimental Fixture. During the past year, the second prototype fixture (labeled Prototype II) was fabricated, tested and evaluated, modified, and reevaluated.

The design of this new two-dimensional, water-sheet nozzle was developed from information obtained through the testing and evaluation of the Prototype I fixture. The goals of the Prototype II design were to reduce the pressure drop in the nozzle inlets and to improve the machinability of the nozzle. The Prototype II fixture was machined from 6061 aluminum to facilitate machining and a higher quality surface finish than the 2024 aluminum used in the first prototype. The Prototype II was fabricated with increased clearances within the nozzle to reduce the pressure drop prior to the nozzle tip, and with added supports to maintain constant gap thickness across the width of the nozzle.

The Prototype II fixture was tested using the same flow settings that were used with the Prototype I. The initial results were promising, and much improved over the performance of the Prototype I. However, the liquid sheet was not completely satisfactory. Further testing of theProtottype II resulted in a gradual deterioration of the quality of the sheet. The sheet was found to be perturbed by rough surface effects within the nozzle. Inspection of the nozzle revealed that the 6061 aluminum oxidized readily in the presence of the water. The oxidation resulted in a substantially increased roughness of the surfaces within the nozzle.

The Prototype II fixture was modified by (1) increasing the thickness of the liquid sheet to minimize sheet perturbations, (2) coating the fixture surfaces with Teflon spray to further smooth the surface and prevent oxidation of the aluminum, and (3) polishing the interior filming lip of the fixture with sub-micron lapping film to reduce surface roughness effects. The increase in the thickness of the liquid sheet reduced the size of the surface imperfections relative to the sheet thickness. The coating of the surfaces with Teflon created a surface that not only resisted oxidation, but also had a high contact angle with the water. Polishing the inner surfaces with sub-micron lapping film produced a mirror-like finish. These modifications improved the quality of the sheet. However, it was evident that the quality of the sheet

7

was still not sufficient to meet the goals of the program. While Prototype II was being modified and tested, a new experimental fixture, Prototype III, was designed and fabricated from INCONEL in order to eliminate oxidation of the inner surfaces. Thicker shims were specified to increase the sheet thickness by a factor of five. The width of the sheet was also increased by 50% from Prototype II to Prototype III to allow for greater ease in taking measurements.

The Prototype III was demonstrated at liquid velocities ranging from 3.3 to 7.4 m/sec, and shear air velocities from 0 to 54 m/sec. The tests were conducted with shear air on both sides of the sheet, and on only one side of the sheet. The sheet thickness for the tests was 508 μm and the sheet width was 38.1 mm. The characteristic measurement obtained during the testing was the distance from the tip of the nozzle to the point at which droplets began breaking off from the sheet.

The results of these measurements, plotted versus the shear air velocity, are given in Figures A.1 and A.2. In Figure A.1, the distance to breakup is plotted versus the air velocity at a series of liquid flow rates. All cases appear to approach an asymptotic value as the air velocity decreases. This is expected as the breakup of the sheet is dependent upon the relative velocity of the liquid sheet and the shear air. As the air velocity decreases, the air- liquid system approaches zero relative velocity, at which point there is no shearing to set up surface waves on the sheet, and therefore, no breakup of the sheet. In theory, as the liquid velocity is increased above the air velocity, the sheet at some point will breakup. The limit for a given liquid velocity is when the air velocity approaches zero. This was not observed during the Prototype III shake-down tests possibly because the water momentum was not sufficiently strong to overcome the nozzle-geometry- induced sheet imperfections. To evaluate this hypothesis, the flow capacity of the system is presently being increased to allow for testing with liquid velocities up to 50 m/sec.

8

A second observation from these tests is that the distance from the nozzle tip for sheet breakup increases as the liquid velocity increases for a given air flow rate. In Figure A.2, the distance from the nozzle tip to the point that droplets break off the sheet is plotted versus the shear air velocity for a liquid velocity of 7.4 m/sec. The two cases are shown: shear air flow on one side of the liquid sheet, and shear air flow on both sides of the sheet. In both instances, the distance from the nozzle tip to the breaking off of the droplets decreases with increasing air velocity. An interesting feature of Figure A.2 is that the distance to breakup is constant for the same total air flow. In other words, in the two-sided flow case, the air velocity is only half the air velocity required in the single-sided case for the same distance to sheet breakup. However, since the breakup described in the model is based upon the relative velocity of the liquid and air, this breakup at low liquid velocity may be due to another cause. That is, the momentum of the air component normal to the liquid sheet may be the dominating factor influencing the breakup, in which case it would be expected that the distance to breakup would be the same for the same total air flow rate.

Future Direction. In our efforts to improve the quality of the liquid sheet, we have come across some new ideas from fixtures used in large scale lasers that flow a two-dimensional sheet of dye solution through the laser cavity. In laser applications, the flow undergoes constant acceleration until the nozzle exit. This is illustrated in Figure A.3. It is anticipated that this modification will provide liquid sheet qualities better than those displayed by the earlier prototypes.

Pulse Visualization System. The pulse visualization system has been successfully demonstrated using a non-UV- optimized imaging lens (Canon 18-108mm 1:2.5 Zoom lens with a 6X zoom ratio). This lens, while satisfactory as a test for the basic system, attenuates the UV signal from the nitrogen laser and can only be used in the visible light range. In addition, the mechanical shutters are not fast enough to

9

stop the action of the sprayed sheet.

The Particle Measuring System custom-made UV lens package will be the permanent imaging system used with the pulse visualization system and is on order. The short pulse duration of the nitrogen laser, coupled with the UV lens package, is ideal for taking sharp, clear pictures of the spray. The laser will be used primarily in the single-shot mode for most of the data collection, so that individual frames can be manipulated by the computer through image enhancement routines. However, for imaging the spray in real-time, without computer enhancement, the system can be run up to 20 Hz, or 20 frames per second. The camera can also be used to film on a continuous basis. When the camera is operating in the continuous filming mode; however, it does not update the image with a high enough frequency to obtain high-resolution pictures of the moving spray.

B. ATOMIZATION THEORY

The effort during this period was aimed at extending the mathematical and numerical model described in the last annual report (see also Rangel and Sirignano, 1988) in order to simulate the behavior of a finite-thickness liquid sheet in contact with a stream of air on each side of it. In this context, we should note that our previous analysis of a single interface represents the limit of an infinitely thick sheet or, more realistically, a case in which the sheet thickness is much larger than the disturbance wavelength and the disturbance amplitude. Linear theory may be used also in the finite-sheet case to predict the initial growth of disturbances on the liquid sheet. Figure B.1 is a schematic of two limiting situations that can be investigated. We first consider cases in which the air streams on either side of the liquid sheet move with the same velocity. In one case shown in Fig. B.1, symmetric waves are studied. In the other case, asymmetric or, more properly, shifted-symmetric waves are considered. Much of the effort during the reported period has concentrated on generalizing linear theory results to be used as the starting point for the numerical

10

calculations.

The situation examined at first consists of a planar liquid sheet of finite thickness in contact, on each side, with a stream of air of thickness much larger than that of the liquid sheet. Briefly, inviscid linear theory reduces the problem to the solution of Laplace's equation in each stream subjected to the interface conditions of continuity of normal velocity and momentum balance. Modal analysis is used to represent the evolution of either interface as:

$$\eta = \epsilon^{\imath \omega t} \sin(2\pi x) \tag{1}$$

Linear theory shows that the shifted-symmetric waves are more unstable and for such a case it predicts a cutoff wavenumber that divides the spectrum into a region of stable waves and a region of exponentially growing waves. This cutoff dimensionless wavenumber is found to be:

$$W_c = \frac{1 + \rho}{1 + \rho \coth(2\pi h/\lambda)} \tag{2}$$

where ρ is the density ratio (air/liquid), h is thickness of the undisturbed sheet and λ is the disturbance wavelength. Two things are immediately verified from Eq. 1. First, the limit $h \to \infty$ yields $W_c = 1$ as corresponds to the single-interface case. Secondly, the limit $h \to 0$ results in $W_c \to 0$ which indicates that the stability of the sheet increases as its thickness is decreased. It should be realized, however, that this conclusion is valid only in the case in which the air has the same velocity on both sides. If this were not the case, an infinitely thin liquid sheet would still be unstable since in such a case the two air streams would approach the limit of a vortex sheet as the liquid thickness approaches zero. As in the one-sided case (infinitely thick sheet), linear theory shows that there is a value of the dimensionless wavenumber that yields the maximum growth rate. This value is:

11

$$W_{opt} = \frac{2(1+\rho)\tanh(2\pi h/\lambda)}{3(\tanh(2\pi h/\lambda) + \rho)} \tag{3}$$

The limit of an infinitely-thick liquid sheet is rapidly approached as h increases and yields the density independent value of 2/3.

Our non-linear investigation is based, as it was in the single-interface case, on the vortex discretization method. It is described in detail by Rangel and Sirignano (1988) and in the previous AFOSR annual report. The existence of a second interface means that a second row of vortices must be considered located a distance h below the first one. This two-fold increase in the number of vortex elements translates into approximately a four-fold increase in computational time. Surface-tension and density-ratio effects are included in the form of an evolution equation for the vortex strength of each interface. Other details of the procedure are basically the same ones described in the previous report and need not be repeated here.

Some results are shown in Figs. B.2. through B.6. These figures show the evolution of disturbances for different configurations of interest. Figure B.2 shows a situation that approaches the infinitely-thick-sheet behavior. Here the disturbance wavelength is one half of the liquid sheet thickness (note that the x and y scales are different) and each interface evolves almost independently of the other. Therefore the rollup proceeds as in that case. When the liquid sheet thickness is reduced so that the disturbance wavelength is twice the liquid thickness (Fig. B.3), the effect of the other interface begins to become noticeable. In the limit of zero thickness the two air streams are stable because they have the same velocity. When surface tension is present, the rollup features are gradually eliminated. At the most unstable case, the liquid sheet evolves as illustrated in Fig. B.4, where it may be argued that two ligaments will be produced for each wavelength. The symmetric case is illustrated in Figs. B.5 and B.6 for two different sheet thicknesses. The rollup features again disappear as the thickness is decreased and only one ligament is formed

12

for each wavelength of the disturbance. Thus, the symmetric mode appears to yield larger liquid ligaments and presumably larger droplets than the shifted-symmetric mode.

Further developments are expected to include a parametrization of the surface-tension and density-ratio effects for the finite-thickness liquid sheet perturbed in the symmetric and shifted-symmetric modes. Extension to the case of the two air streams moving with different velocities should follow. By studying the non-linear evolution of these disturbances, it is hoped that some inferences will be made as to what the size of the characteristic ligaments is and what effects the various different parameters have on this size.

C. TURBULENT REACTIVE FLOWS

The analysis of concentration distributions in a non-reacting shear layer continued during this reporting period. In this new effort, the investigation focused on the problem of the interaction of a vortical flow with molecular species diffusion, considering the situation where an infinite row of two dimensional vortices is superposed onto an interface initially separating two species. Under the action of the vortical field, layers of both fluids tend to roll up as shown in Fig. C.1.

The level of resolution required to quantify the molecular diffusion process results in highly time consuming computations. Because of this, an approximate analytical approach based on the methodology of Marble (1985), Karagozian (1982), and Karagozian and Marble (1986) is employed to solve the temporal growth of the mixing layer locally. This approach was recently used by Cetegen and Sirignano (1987,1988) to determine the concentration field and probability density functions using Taylor's frozen flow assumption. This analysis has been extended to construct the pdf in a laboratory frame of reference, providing ways for a more realistic

13

comparison with results of mixing layer experiments reported in the literature (Dimotakis, 1986; Dimotakis and Brown, 1976; and Masutani and Bowman, 1986).

The velocity field for an infinite row of equidistant two dimensional vortices (Lamb, 1945) was modified to account for a viscous core in cases of one, three, or five vortices. Consideration of more than five viscous vortices proved unnecessary, as it is reported by Miralles-Wilhelm et al (1989). A nondimensional vortex strength, represented by the Reynolds number, $Re = \Gamma/2\pi\nu$, evolves form this analysis as an important parameter governing the process.

An analytical solution of the conservation of species equation for a material element located instantaneously at the interface separating the two non-reacting species can be written in terms of an error function of appropriately stretched distance and time coordinates, accounting for the strain history of each material element. The nondimensionalization of this equation introduces the Schmidt number $Sc = \nu/D$ as the parameter controlling the molecular diffusion process. The strain rate is computed locally from the velocity field and the shape of the interface.

Figure C.2 shows the distortion of the initially horizontal material line separating the two species at certain instants after the vortices are initiated. The aging process of the vortices is taken into account, since the vortices are born periodically in time. Notice that as time passes, the roll up of layers of the fluid streams is augmented.

Figure C.3 shows the time evolution of the concentration profile for the single vortex case (Re=50;Sc=1), as it would be measured by a probe located at different heights above the mixing plane originally dividing the two species. Notice that as the height y of the probe decreases approaching the mixing plane, a well mixed region is encountered (i.e. the vortex core). It is in this region where the diffusion

14

process occurs more efficiently, as expected. On the other hand, when the height of the probe increases, an increasing tendency towards non-mixing can be observed, until no mixing at all is reached far away from the vortex center. In a frame of reference attached to the vortical center, it has been shown that the concentration profiles exhibit an antisymmetry (Cetegen and Sirignano, 1987, 1988). That antisymmetry is not found in Figure C.3, for a frame of reference that is fixed, as in an experimental situation. It is from these curves that the probability density function at different y locations is constructed. Figure C.4a shows the pdf for the case described above. As it was noted before, the higher peaks correspond to the unmixed concentrations far away from the vortex center, and finite probabilities of intermediate concentrations exist in the vortex core region, as it is shown by the other relative smaller peaks.

The numerical results for the frozen flow approximation exhibit a characteristic antisymmetry whereby $pdf(y, C) = pdf(-y, 1 - C)$, while experimental evidence shows that the peaks that occur in the high speed stream side of the flow are greater than those on the low speed stream side. For this reason, the relative difference R between the pdf at a given (y, C) pair and its antisymmetrical counterpart $(-y, 1 - C)$ is plotted in Fig.C.4b. The numerical calculations and the shape of the graph reveal three important facts. First of all, that R can be nonzero and therefore antisymmetry is not found. Secondly, the pdf peaks for the high speed stream are not always greater than those for the low speed stream (R can be a negative quantity). The other important issue showed by this graph is that the absolute value of R is much greater when R is positive. This means that when the peaks in the high speed stream are greater than those on the low speed stream, the relative difference between them is much greater (of the order of 5 times) than that in the opposite case (when the low speed stream peaks are higher than the high speed stream ones). This last result tends to agree with the experimental results presented by Masutani and Bowman (1986), while the first results support the idea that these experimental

15

results (R always positive) are a consequence of the measurement bias, rather than a result of a real difference in mixing rate. The high speed side of the vortical structure moves faster on average towards the probe than the low speed side, so that the probe sees a different concentration profile and a different pdf from that seen in a frame of reference attached to the vortical structure. A theoretical explanation of the influence of a Galilean transformation on the pdf is given by Miralles-Wilhelm et al (1989).

The influence of Re and Sc on the mixing process can be presented in terms of a local or averaged mixedness parameter, given by Miralles-Wilhelm et al (1989) and Cetegen and Sirignano (1987), respectively. In both cases, an increase in Re, enhances the mixing process by increasing the rolling up of the fluid layers into each other. Also, in both cases, a weak dependence on Sc is observed. This results, presented by Miralles-Wilhelm et al (1989) are in agreement with those presented by Cetegen and Sirignano (1987). In a frame of reference attrched to the vortical structure, an antisymmetric pdf results, and thus the mixedness results for +y and -y collapse into one curve, as observed in Fig. C.5.a. The presence of the surrounding vortices tend to decrease the rate of mixing away from the mixing plane, which subsequently diminishes the overall mixing process. This is shown in Fig C.5.b.

In conclusion, both an increase in the Reynolds number and a decrease in the Schmidt number tend to increase the probabilities in the mixed core region. That is, the mixedness in the layer is greatly enhanced by increasing the vortical strength, and its relatively poorly influenced by molecular diffusion. The pdf computations relaxing the frozen flow assumption suggest that the bias present in experimental results is not caused by differences in mixing rate. It is not a mixing bias, it is a measurement bias. This fact can be explained theoretically, based on a conservation principle, as shown in the work of Miralles-Wilhelm et al (1989).

The second part of the work carries the study of the mixing phenomena just described into situations in which the fluid dynamics are more complex. Specifically, the intention is to examine the process of molecular mixing when it occurs during the formation of coherent structures (vortex rollup) and during the pairing and merging of vortical structures as it takes place, for example, in a mixing layer.

The inviscid fluid dynamics of vortex pairing and merging is investigated in two different situations employing the method of vortex dynamics (Rangel and Sirignano, 1989). The first situation considers the pairing and merging of isolated vortical structures and of vortical structures in a shearing flow. Thus, the mechanism of pairing is analyzed in an idealized fashion. The second situation considers vortex rollup and pairing of two or grouping of more of these structures when there is an initial surface of discontinuity or vortex sheet separating two streams traveling at different velocities. The temporal instability of this vortex sheet is an approximation to the temporal and spacial instability occurring in a turbulent mixing layer.

The method of solution employed in this study is based on the dynamics of vorticity motion. Generally, these methods take advantage of the fact that in many flows, vorticity is concentrated in regions which are small compared to the total flow domain. The evolution of the vorticity field can then be obtained by solving a system of dynamic equations for a large number of representative vortex cylinders. The use of finite-core vortex cylinders was introduced by Chorin and Bernard (1972) as a means of reducing the numerical instability inherent to this problem.

In an idealization, the mixing layer may be conceptualized as an infinite vortex sheet subjected to a certain disturbance. The disturbance grows to produce the finite vortical structures while the mechanism of viscous diffusion spreads the vorticity on the smaller length scale. The interaction of these vortical structures, induced by the existence of subharmonics of the initial disturbance, results in the pairing and merg-

17

ing of the structures. In the inviscid limit, the vortex sheet rolls up so that singular concentrations of vorticity with one wavelength spacing are formed. If subharmonics exist, these vortical structures interact and pairing can occur (Ho and Huang, 1982).

An isolated vortex line in a two-dimensional inviscid flow produces a circular flow pattern where the circulation along any closed path containing the vortex line is a constant. When two of these vortex lines are located a certain distance apart, the resulting motion is such that the two vortex lines rotate with constant velocity about the point located at the center of the segment joining them (Batchelor, 1970). The separation distance remains fixed so that no merging occurs regardless of the separation. This is an indication that such a concentration of vorticity does not lead to merging. If the vorticity is not initially concentrated along a line but confined inside a cylinder of finite cross section, merging is possible as will be shown below. The initial distribution of vorticity over a circular cross section can be conceptualized as made up of cylindrical tubes (rings in the cross sectional area), so that the total vorticity is the sum of the contribution of all rings. The interaction of two such vortex tubes, one from each vortex cylinder is show in Fig.C.6. Rotation is in the clockwise direction. The characteristic length used in the nondimensionalization is the radius of the ring, while the characteristic time is a circulation time formed with the characteristic length and the circulation. The number of elements employed in the calculation is entered at the upper right corner of each frame as n and all the calculations are started with n=20. For the case illustrated in Fig.C.6, the ring separation from center to center is two ring diameters. As seen in this figure, this separation is small enough so that mutual attraction occurs leading to merger of the two rings. For sufficiently large separation (more than four diameters from center to center), each ring perceives the other ring essentially as a line vortex and neither attraction nor merging occurs. In a developing mixing or shear layer, there is a spacial evolution of the vortical structures in the direction of the flow. At a given time, the downstream structures are older and therefore larger than the upstream

18

ones.

The behavior of two structures of different size is presented in Fig.C.7 for two structures of the same total circulation but of a size ratio of 2/3. This is an idealization of the effect of viscous diffusion, which would tend to spread the vorticity. thus reducing its strength but conserving the total circulation. As seen in Fig.C.7, the smaller structure is eventually entrained by the larger one. This behavior should be of significance in the mixing of a passive scalar or two reactive species, as a structure containing one of the reactants may be trapped inside another structure containing the other reactant thus affecting the rate of reaction.

In a shear layer, the vortical structures may be initially so far apart that they perceive each other as point vortices. Eventually they would grow as a result of viscous diffusion but this mechanism alone is not sufficient to effect a fast merging of two or more structures. It is the shearing action that is responsible for bringing the structures closer together. To visualize this effect we consider two vortical tubes initially separated by a distance of four tube diameters. Such an arrangement would not produce pairing and merging because, as explained above, the structures are sufficiently far apart. In a shear layer, however, these two structures are not alone. Assuming that only the most unstable disturbance is present, without any subharmonics, there would be one such structure every wavelength along the layer. In this case the wavelength is equal to the separation distance. For the purpose of this visualization, all the other vortical structures are represented as fixed line vortices. The two vortex tubes are initially displaced a small amount which is positive for the structure on the left and negative for the structure on the right. Figure C.8 shows the evolution of the two central vortex tubes under the influence of the infinite row. Initially, the two structures move slowly towards each other. After a dimensionless time of 400, the close range interaction leading to pairing begins, resulting in the merged structure shown in the last frame.

19

The rollup, pairing, and merging of vortical structures formed during the evolution of an inviscid vortex sheet subjected to a sinusoidal disturbance and one or more of its subharmonics has also been investigated. In this case, the surface of discontinuity is discretized into a large number of vortex lines. A sinusoidal disturbance and any desired subharmonics are then applied to the interface. Acton (1976) studied the evolution of the inviscid vorticity field using vortex dynamics. Since no rediscretization or insertion of new vortices was performed, the structure of the eddy was lost once it was formed. With the method employed here, the initial resolution can be maintained to the extent of the calculation. In the following figures, lengths have been made dimensionless with the disturbance wavelength, while time has been made dimensionless with a residence time defined as the ratio of the wavelength to the magnitude of the velocity discontinuity at the undisturbed interface. Figure C.9 illustrates a situation in which a sinusoidal disturbance and its first subharmonic, both of dimensionless amplitude 0.025, are simultaneously imposed on the interface at t=0. The number of vortex elements n is indicated at each time frame. Figure C.9 shows how the presence of the first subharmonic forces the pairing of every two structures in the manner described in the experiments of Ho and Huang. No complete merging occurs because there is no diffusion mechanism present to spread the vorticity away from the interface. Figure C.10 shows the results for a case in which the second subharmonic is present in addition to the fundamental. In this case, grouping of every three structures occurs and most importantly, the transverse thickening of the layer occurs more rapidly since there are now three structures rolling up together (Note that the x and y scales in Fig. C.10 are different from those of Fig. C.9). The evolution of the vorticity distribution for the case of Fig. C.10 is shown in Fig. C.11, where the vortex strength (circulation per unit area) is plotted against a coordinate along the interface. The rollup of vorticity into three structures is apparent in this figure as well as the absence of viscous diffusion and merger.

Figure C.12 shows the amplitude of the disturbance as a function of time for the case of a single disturbance, a disturbance plus the first subharmonic, and a disturbance plus the second subharmonic. The exponential growth rate predicted by the linear theory is valid until a dimensionless time of 0.8 approximately. From then on, the single-disturbance grows slowly to a maximum and then actually decreases due to the strong shear generated by the resulting vortex row and the absence of viscous diffusion. The cases containing the first and second subharmonics continue to grow nearly linearly until a dimensionless time of 3. From this point on, the case containing the first subharmonic reaches a maximum amplitude and then decreases also due to the absence of merger in the presence of strong shear. The amplitude of the case containing the second subharmonic continues to grow linearly although at a faster rate induced by the three structures that begin to roll up together.

D. VAPORIZING-DROPLET CALCULATIONS

The detailed analysis of a vaporizing droplet in the convective field with variable thermo-physical properties has been examined in Chiang. Raju and Sirignano (1989). We present here some of the results of our recent study. The base case study is selected as a cold n-octane fuel droplet suddenly injected into the hot gas stream. The values of physical parameters in the base case are given in Table D-1. Several parameter studies by changing initial droplet temperature, ambient temperature. initial Reynolds number, and droplet heating model are also made to investigate the effect of the above quantities.

Typical contour plots of mass fraction, temperature, vorticity as well as liquid-phase streamlines and the gas-phase velocities are presented in Figure D. 1. The convective effect is apparent by the fore-aft asymmetry in each plot. We may observe the gas-phase boundary layers surrounding the droplet up to 136° in angular direction and a near wake region behind the droplet. The vorticity contours are con-

centrated at the front portion of the droplet and then are convected downstream. The temperature and mass fraction contours do show the presence of the boundary layer and wake. However, they are not similar to each other because of non-unitary Lewis number. The liquid-phase streamlines show a single large vortex, roughly resembling a Hill's spherical vortex, in the interior of each droplet. The similarity between the isotherms and streamlines in the liquid phase shows the influence of internal circulation.

The surface shear stress distribution shown in Figure D. 2.a indicates the shear stress decreases with time. This can be realized by the following facts: (1) With the onset of surface motion, the velocity gradient at the droplet surface decreases. (2) The surface blowing effect, which increases the thickness of the boundary layer and reduces the velocity gradient, is growing as vaporization becomes stronger. (3) As droplet heating continues, the mass fraction at the surface also keeps increasing, thus yielding lower values of viscosity of the mixture.

The tangential velocity distribution shown in Figure D. 2.b seems to vary with $sin\theta$ which is in qualitative agreement with Hill's vortex solution. The surface tangential velocity, originally zero, is brought up to a maximum by the shear stresses and then decreases as shear stresses diminish.

The distribution of vorticity along the droplet surface is very similar to that of shear stress as shown in Figure D. 2.c The surface vorticity is obtained from

$$\omega_l = \frac{\mu'_g}{\mu'_l}[\frac{\partial}{\partial n}V_{g,\theta} - \frac{V_{g,\theta}}{a} + \frac{1}{a}\frac{\partial}{\partial \theta}V_{g,n}]_s - 2\frac{\partial V_{l,\theta}}{\partial n}|_s \tag{4}$$

The dominating term is $\frac{\partial}{\partial n}V_{g,\theta}$ which is also the main term contributing to the shear stress. It is clear that $\omega \sim \frac{1}{\delta} \sim Re_g^{1/2}$. Hence it is expected that the effects of internal circulation, boundary layer blowing and reduction of gas-phase Reynolds number will cause the surface vorticity to diminish. If the flow separation point is

determined by the point where vorticity changes sign. it is observed that the separation point is approximately located around 144 degrees.

Figure D. 2.c shows the pressure distribution. The recirculating wake dissipates part of the kinetic energy. As a result , the pressure cannot recover to the stagnation value. We now switch our attention to the overall characteristics of momentum. heat and mass transfer to the droplet. Figure D. 3 shows the variation of drag coefficients of droplets initially at three different ambient temperatures as a function of hydrodynamic diffusion time. Also shown in this figure is the drag correlation of Renksizbulut and Haywood (1986) which is based on the numerical results of an isolated moving drop. vaporizing in its own fuel-vapor medium: their analysis also considers the effect of variable thermophysical properties. The R-H correlation is given by.

$$C_D(1 + B_{H,f})^{0.2} = \frac{24}{Re_m}(1 + 0.2Re_m^{0.63}); 10 \leq Re_m \leq 300 \qquad (5)$$

where

$$B_{H,f} = \frac{C_{p,f}(T_\infty - T_s)}{L_s}(1 - \frac{Q_l}{Q_g})$$

The time required for the flowfield to relax from the initially impulsive motion. due to the sudden injection of the drop into a uniform flowfield, can be estimated as $\Delta t_{relax} \sim \frac{2R_\infty}{U_\infty} \sim 0.4$ of the diffusion time. During the initial relaxation period the drag coefficient falls rapidly. Subsequently C_d increases as a result of a reduction in the Reynolds number. However for the higher ambient temperature case where the large heat flux makes droplet vaporization grow rapidly during the early portion of life time, the drag coefficient is therefore significantly decreased due to the boundary layer blowing. For all cases, C_d tends to increase with time during the final portion of the calculation which implies that the reduction in Reynolds number takes control in determining drag coefficients. The R-H drag correlation seems to be not applicable in our cases, except at the early times of the lower transfer number

23

case (ambient temperature = $800°K$) where the vaporization is weak. The deviation becomes large for the high transfer number case.

Three components of drag coefficients are shown in Figure D. 3. It is clear that the major differences in total drag coefficients for three different ambient temperature cases are resulting from differences in the friction drag coefficient. A higher transfer number can reduce the friction drag by a large amount. The thrust drag is always negligible and at most accounts for less than 2% reduction of the total drag. The pressure drag coefficients increase steadily which may be due to the increase of the wake's strength as the vaporization increases with time.

Figure D. 4.a shows the average Nusselt numbers of these three cases and their corresponding R-H Nusselt number correlations which can be expressed as

$$Nu_f(1 + B_{H,f})^{0.51} = 2 + 0.68 Re_m^{1/2} Pr_f^{1/3}$$

The Nusselt number falls during the initial relaxation period. Further reduction in the Nusselt number is believed to be attributed mainly to a Reynolds number reduction and an increase of surface blowing. Again our numerical results do not agree with the R-H correlation as in the drag calculation. However the discrepancy becomes smaller during the final calculation when the surface temperature approaches the wet-bulb temperature. The discrepancy in both C_d and Nu number between our calculation and R-H's calculation may be attributed to the different definition of the problem considered. In their calculation. R and H considered a droplet vaporizing in its own fuel-vapor environment. As a result, the mass diffusion was neglected. In addition, they keep constant droplet surface temperature at the boiling point which may reduce the heat transfer from the gas-phase and may cause quite different thermophysical properties at the interface when compared to our calculation.

24

The Sherwood number, which represents the transient dynamics of the mass transfer, is shown in Figure D. 4.b. The general trend of variation is very similar to that of Nusselt number. During the early relaxation period, the large mass fraction gradient caused by the suddent injection of a droplet to the hot gas-stream is smeared out gradually. This relaxation contributes mainly to the early reduction of Sherwood number. A more general decrease of Sherwood number is then observed, which may be due to the decay of Reynolds number.

In order to study the effect of initial droplet temperature, the initial droplet temperature has been raised from $300K$ to $400K$. The results are shown in Figure D. 5.a It is very clear that for the higher initial droplet temperature case, the surface blowing effect is more significant than that of the lower droplet temperature case during a large portion of the droplet life time. Hence the former experiences lower drag than the latter. Figure D. 5.b shows the portion of total heat flux that goes into heating of the drop interior. The droplet with higher initial temperature would spend most of the available heat energy in evaporation process. On the contrary, the droplet with lower initial temperature has to spend most of the available energy to heat up itself first, with the remaining energy going for vaporization. As a result the heating process is slow and will persist for most of the lifetime. The vaporization is also relatively weaker compared to the high initial temperature droplet. Also shown in this figure is the solid sphere correlation which can be grossly inaccurate due to the high mass transfer at the surface.

The effect of variable thermophysical properties is always interesting for the range of temperatures considered in the present study. A calculation has been conducted by assuming constant properties that are based upon the values in the far stream. Since the global behavior is evaluated at the interface where the mixture constituent is very different than the pure gas in the far stream. The results in Figure D. 6 show that the constant-property calculations result in the overprediction of

the drag coefficient by about 20%. The discrepancy is attributed to the change in thermo-physical properties at the interface and the change in the flow field caused by the property gradients.

The effect of initial Reynolds number was also studied during the current work. The calculations for three different initial Reynolds numbers have been made. The results are presented in Figure D. 7. It is observed that lower initial Reynolds number results in a higher drag coefficient at early times due to the smaller convective momentum transport which usually causes the early separation to occur. It is also noteworthy that the three drag coefficients at the final calculation tend to approach a certain form which is governed by the reduction in Reynolds number only.

The droplet model is very important to combustor design. Figure D. 8 show the comparison results from an infinite conductivity liquid-phase model where the liquid-phase temperature is assumed to be uniform in space but varying with time. The results indicate that the infinite conductivity case predicts higher drag in the early part of the droplet lifetime and lower drag later on. For the infinite conductivity model, the liquid phase has to distribute all the available heat flux to the droplet interior. Thus the surface temperature rises slowly resulting in very weak vaporization rate as well as in a high drag coefficient during the early lifetime. Because of the larger driving temperature potential, the droplet eventually receives more heat flux than that calculated from our model. As a result, the surface temperature builds up and the vaporization grows quickly while the drag coefficient is reduced significantly.

With the results of above cases, it is desirable to obtain the correlations of drag coefficient, Nusselt numbers as the function of some important parameters. Since these transport quantities are determined by the combined influence of surface blowing and vaporization, the internal circulation, and the unsteady effects related to the droplet deceleration. A complete correlation which covers a wide range of

26

all parameters is not easy to achieve. The parameters and functional form selected in this work are the same as in the R-H's correlation. The following modified correlations show a good agreement (within 3% discrepancy) in our results as shown in Figure D. 9

$$C_D(1 + B_{H,film})^{0.336} = \frac{24}{Re_m}(1 + 0.225Re_m^{0.61})$$

$$Nu_{film}(1 + B_{H,film})^{0.51} = 2 + 0.6Re_m^{1/2}Pr_{film}^{1/3}$$

for $.6 \leq B_{H,film} \leq 6/and30 \leq Re_m \leq 250$

The major difference between the our modified correlation and R-H correlation is the exponent of $(1 + B_{H,film})$. Our correlation has a higher exponent which emphasizes more reduction in drag coefficient by the effect of transfer number.

The droplet interaction effects are determined by the combined influence of surface blowing and vaporization, the internal circulation, and the unsteady effects related to the droplet deceleration. Since the problem contains a multidimensional variable space, an exhaustive numerical study of all possible combinations of parameters would be extremely elaborate. Therefore, we have concentrated our attention in detailed study of the interaction effects rising from the variation of Reynolds number $Re_{g,0}$, initial diameter ratio $a'_{2,0}/a'_{1,0}$, and initial spacing to lead droplet diameter ratio d_0. Most of the results are presented in Raju and Sirignano (1987, 1988). The main observations from this research can thus be summarized as follows.

Droplet collision appears to be likely for the initially equal-sized droplets, as long as the initial spacing is sufficiently small for the wake effects to be important. However, the decrease in the downstream drop size can prevent collision since droplet deceleration is inversely proportional to its radus. The results indicate that there exists a bifurcation point depending upon the critial ratio of $a'_{2,0}/a'_{1,0}$ below

27

which droplet collision becomes unlikely; the smaller the ratio, the faster the rate at which drops separate from each other; the larger the ratio, the faster the rate at which drops approach each other. Closer to the bifurcation point, the droplets spend more time under the influence of each other before either droplet cllision or separation eventually occurs. Larger initial Reynolds numbers as well as smaller initial droplet spacing tend to reduce the critical downstream drop size required for droplet separation. The time required for droplets to collide is relatively insensitive to the Reynolds number.

The lead droplet experiences higher drag force than the downstream droplet which is shielded by the lead droplet. The lead droplet behaves as an isolated vaporizing drop as long as the two drops are separated sufficiently $(2 \leq d)$. After studying some cases the drag coefficients of the two droplets can be correlated by

$$C_{d,2} = (\frac{V_{\infty,1}^2}{V_{\infty,2}^2})(\frac{a_2}{a_1})C_{d,1} - 1.22(\frac{a_2}{V_{\infty,2}^2})d_0^{-0.25}Re_{g,0}^{-0.18} \tag{6}$$

The numerical results satisfy the above equation within 8 percent accuracy for the range of initial spacings between 2-15 and initial Reynolds numbers between 50-200.

Figure D. 10 shows the overall Nusselt numbers Nu and average surface temperature T_s for the case of two approaching droplets. The difference in both Nu and T_s between two droplets indicate that wake effects tend to reduce significantly the heat transport to the downstream drop. For the case of separating drops, the Nusselt number for the downstream drop during the final period of calculation approaches the theoretical value for an isolated droplet as shown in Figure D. 11.

While a general understanding is obtained through a parametric study of the interaction effects between two vaporizing droplets, the results are by no means conclusive, e.g., particle dynamics may be quite different if a very small particle gets trapped in the standing eddy of the lead droplet. Further studies are needed for a

complete understanding of the drop behavior near the bifurcation point. The present analysis does not allow for droplet coalescence, or atomization. Future studies of the dynamics during collision would be worthwhile. The interactive droplets must also be studied with variable properties and general (three-dimension) orientation.

IV. REFERENCES

Marble, F.E., Growth of a Diffusion Flame in the Field of a Vortex. *Recent Advances in the Aerospace Sciences*. pp. 395-413. Editor: Corrado Casci. Plenum Publishing Corporation (1985).

Karagozian. A.R., An Analytical Study of Diffusion Flames in Vortex Structures. Ph.D. Thesis. California Institute of Technology (1982).

Karagozian. A.R. and Marble. F.E., Study of a Diffusion Flame in a Stretched Vortex. *Combustion Science and Technology*. Vol. 45. pp. 65-84 (1986).

Rangel. R.H. and Sirignano. W.A., The Dynamics of Vortex Pairing and Merging. AIAA 27th Aerospace Sciences Meeting. AIAA 89-0128. Reno, Nevada (1989).

Cetegen, B.M. and Sirignano, W.A., Study of Mixing and Reaction in the Field of a Vortex. Joint Meeting of the Combustion Institute Western States and Japanese Sections, Paper No. 3B-44, Honolulu, Hawaii (1987).

Cetegen, B.M. and Sirignano, W.A., Study of Molecular Mixing and a Finite Rate Chemical Reaction in a Mixing Layer, *Twenty-Second Symposium (International) on Combustion*, Seattle, WA, August 1988. Also see Analysis of Molecular Mixing and Chemical Reaction in a Mixing Layer, AIAA 26th Aerospace Sciences Meeting. AIAA 88-0730, Reno, Nevada (1988).

Dimotakis, P.E., Two-dimensional Shear-Layer Entrainment, *AIAA J.*, 24. pp. 1791-

1796 (1986).

Dimotakis, P.E. and Brown, G.L., The Mixing Layer at High Reynolds number: Large Structure Dynamics and Entrainment, *J. Fluid. Mech.*, 78, pp. 535-560 (1976).

Masutani, S.M. and Bowman, C.T., Structure of a Chemically Reacting Mixing Layer. *J. Fluid. Mech.*, 172, pp. 92-126 (1986).

Lamb, H., *Hydrodynamics*, Chapter VII, Sixth Edition, Dover Publications, New York (1945) 25th Aerospace Sciences Meeting, AIAA 87-1224, Reno, Nevada (1987).

Miralles-Wilhelm, F., Rangel, R.H. and Sirignano, W.A., An Analysis of Molecular Mixing in a Vortical Structure: Bias in PDF measurement, AIAA 27th Aerospace Sciences Meeting, AIAA 89-0482, Reno, Nevada (1989).

Chorin, A. J. and Bernard, P. S., Univ. of California, Berkeley Engng. Rep. FM-72-5, (1972).

Ho, C-M. and Huang, L-S., Subharmonics and Vortex Merging in Mixing Layers, *J. Fluid Mech.*, 119, 443-473, (1982).

Batchelor, G. K., *An Introduction to Fluid Dynamics*, Cambridge University Press, (1970).

Acton, E., The Modelling of Large Eddies in a Two-dimensional Shear Layer, *J. Fluid Mech.*, 76, 561-592, (1976).

Chiang, C. H. , Raju, M. S. and Sirignano, W. A. (1989). Numerical Analysis of Convecting, Vaporizing Fuel Droplet with Variable Properties, AIAA Aerospace

Sciences Meeting. Paper 89-0834.

Haywood, R.J., and Renksizbulut, M., On Variable Property. Blowing and Transient Effects In Convective Droplet Evaporation with Internal Circulation, *Proceedings of the Eighth International Heat Transfer Conference*, pp. 1861-66, 1986.

Raju, M.S. and Sirignano, W.A. Interaction Between Two Vaporizing Droplets in an Intermediate-Reynolds-Number-Flow, submitted to *Physics of Fluids*.

V. PUBLICATIONS

Rangel, R.H. and Sirignano, W.A., Combustion of Parallel Fuel Droplet Streams, accepted by *Combustion and Flame*, 1988. Also see Vaporization, Ignition, and Combustion of Two Parallel Fuel Droplet Streams, Proceedings of the 1987 ASME-JSME Thermal Engineering Joint Conference, Vol. 1, pp. 27-34, Honolulu, HI, March 1987.

Raju, M.S.and Sirignano, W.S., Interaction Between Two Vaporizing Droplets in an Intermediate-Reynolds- Number-Flow, submitted to *Physics of Fluids*, 1987. Also see Unsteady Navier-Stokes Solution for Two Interacting Vaporizing Droplets, AIAA Preprint No. 87-0300, Reno, NV, January 1987.

Rangel, R.H. and Sirignano, W.A., Non-Linear Growth of Kelvin-Helmholtz Instability: Effect of Surface Tension and Density Ratio, *Physics of Fluids*, V. 31, pp. 1845-1855, 1988. Also see Atomization of Liquid Fuels: Non- Linear Growth of Disturbances at an Interface, Spring 1987 Western States/ Combustion Institute Meeting, Provo, UT, April 1987.

Cetegen, B.M. and Sirignano, W.A., Study of Molecular Mixing and a Finite Rate

Chemical Reaction in a Mixing Layer, *Twenty-Second Symposium (International) on Combustion*, Seattle, WA, August 1988. Also see Analysis of Molecular Mixing and Chemical Reaction in a Mixing Layer, Preprint No. 88-0730, AIAA 26th Aerospace Sciences Meeting, Reno, NV, January 1988.

Rangel, R.H. and Sirignano, W.A., Unsteady Flame Propagation in a Spray with Transient Droplet Vaporization, *Twenty-Second Symposium (International) on Combustion*, Seattle, WA, August 1988. Also see Unsteady Flame Propagation in a Two-Dimensional Spray with Transient Droplet Vaporization, Preprint No. 88-0641, AIAA 26th Aerospace Sciences Meeting, Reno, NV, January 1988.

Cetegen, B.M. and Sirignano, W.A., Study of Mixing and Reaction in the Field of a Vortex, presented at the Joint Meeting of the Western States Section/Japanese Section of The Combustion Institute, Honolulu, HI, November 1987. To be submitted for publication in *Combustion Science and Technology*.

Miralles-Wilhelm, F., Rangel, R.H., and Sirignano, W.A., An Analysis of Molecular Diffusion in a Vortical Structure: Bias in PDF Measurement, Preprint No. 89-0482, AIAA 27th Aerospace Sciences Meeting, Reno, NV, January 1989.

Rangel, R.H. and Sirignano, W.A., The Dynamics of Vortex Pairing and Merging, Preprint No. 89-0128, AIAA 27th Aerospace Sciences Meeting, Reno, NV, January 1989.

Chiang, C.-H., Raju, M.S., and Sirignano, W.A., Numerical Analysis of Convecting, Vaporizing Fuel Droplet with Variable Properties, Preprint No. 89-0834, AIAA 27th Aerospace Sciences Meeting, Reno, NV, January 1989.

VI. PRESENTATIONS

Workshop on Experimental. Analytical and Computational Methods in Liquid Fuel Sprays, a series of three lectures at the Institute of Aeronautics and Astronautics. National Cheng Kung University, Tainan, Taiwan, November 1987.

Mixing and Reaction in a Vortical Structure, UC San Diego, March 1988.

Review of Spray Combustion Theory: Remaining Challenges on the Droplet Scales. Workshop on Mass, Momentum, and Energy Exchange in Combusting Sprays: Droplet Studies, Sandia National Laboratories, Livermore, CA. March 1988.

Fundamental Studies on Spray Combustion and Turbulent Combustion, 1988 AFOSR/ONR Contractors Meeting on Combustion, California Institute of Technology, Pasadena, CA. June 1988.

Analysis of Vortical Stuctures in Combustion Processes. Invited Seminar, Department of Mechanical and Aerospace Engineering. Princeton University, October 1988.

VII. LIST OF PROFESSIONAL PERSONNEL
C.-H. Chiang, Research Assistant, Ph.D. Candidate
F. Miralles-Wilhelm, Research Assistant, M.S. Candidate
M.S. Raju, Research Associate. Departed
R.H. Rangel, Research Associate
G.S. Samuelsen, Professor, Co-Principal Investigator
W.A. Sirignano, Professor, Co-Principal Investigator
W.A. Sowa, Associate Director, Combustion Laboratory
B.E. Stapper, Research Assistant
H.D. Crum, Developmental Technician

Table D-1. Values of Physical Parameters Used in Base Case Computation
for Variable Property Single Droplet

Parameter	Value
Initial Reynolds number, gas phase $Re = 2a'_0 U'_{\infty,0} \rho'_{g,\infty} / \mu'_\infty$	100.0
Relative velocity of drop, m/s	25.0
Free stream temperature, °K	800.0
Combustor pressure, atm	10.0
Prandtl number, gas phase	0.799
Prandtl number, liquid phase	9.32
Schmidt number, gas phase	2.23
Molecular weight, oxidizer, Kg/Kmol	29.0
Molecular weight, fuel, n-octane, Kg/Kmol	114.2
Droplet initial temperature, °K	300.0
Viscosity ratio, $\mu'_l / \mu'_{g,\infty}$	9.30
Density ratio, $\rho'_l / \rho'_{g,\infty}$	362.47
Specific heat at constant pressure ratio, $C'_{pl,0} / C'_{pg,\infty}$	1.69
Latent heat / Specific heat of liquid, °K	136.8
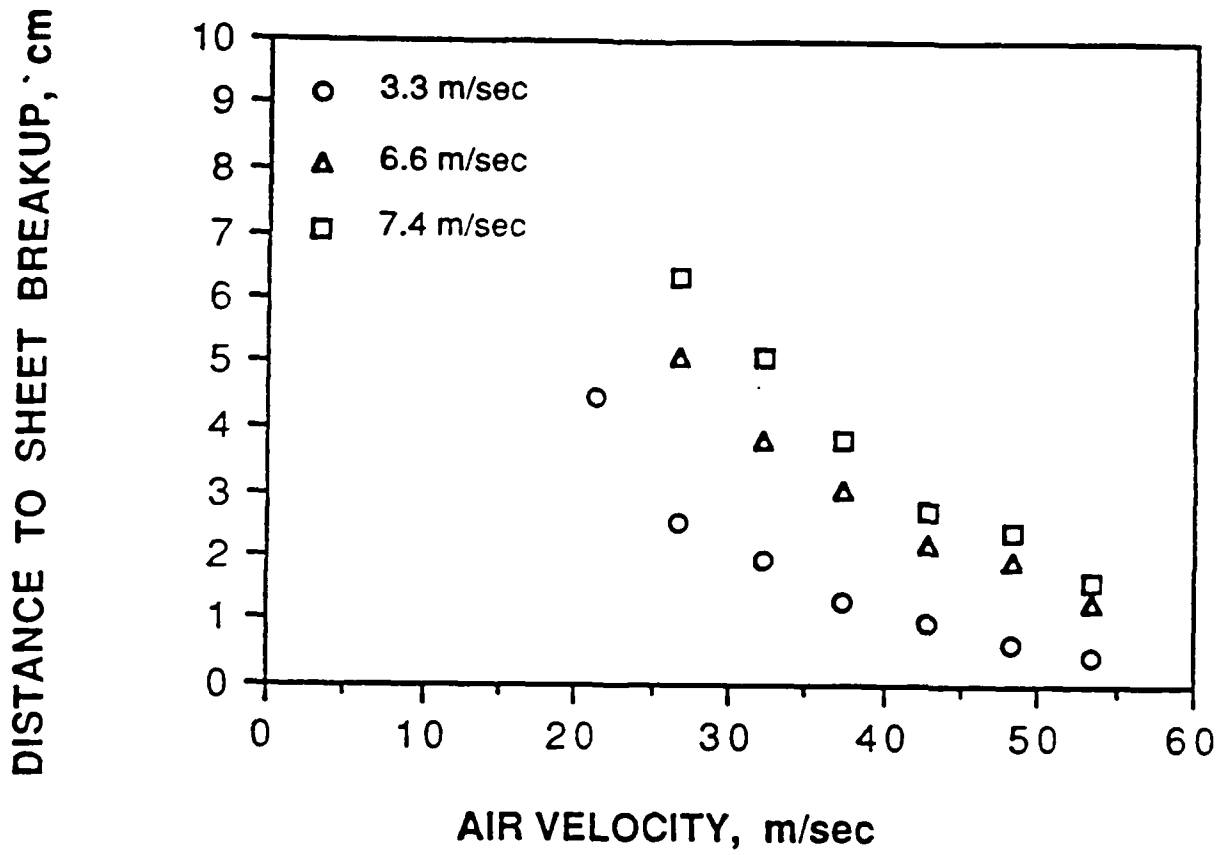
FIGURE A-1. Plot of Distance to Breakup versus Shear Air Velocity for Various Liquid Velocities.
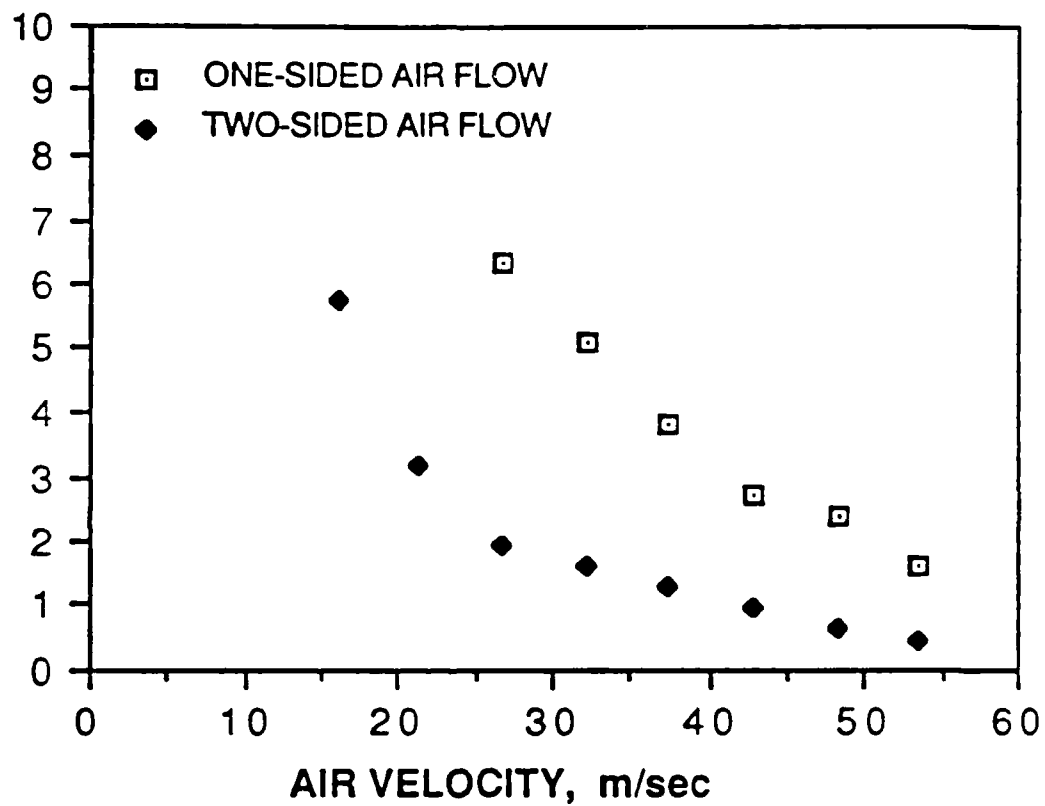
FIGURE A-2   Plot of Distance to Breakup versus Shear Air Velocity for One
and Two-Sided Shear Air Flow.

—————— PRESENT DESIGN

·········· PROPOSED MODIFICATION

Liquid Flow

Shear Air Flow

Shear Air Flow
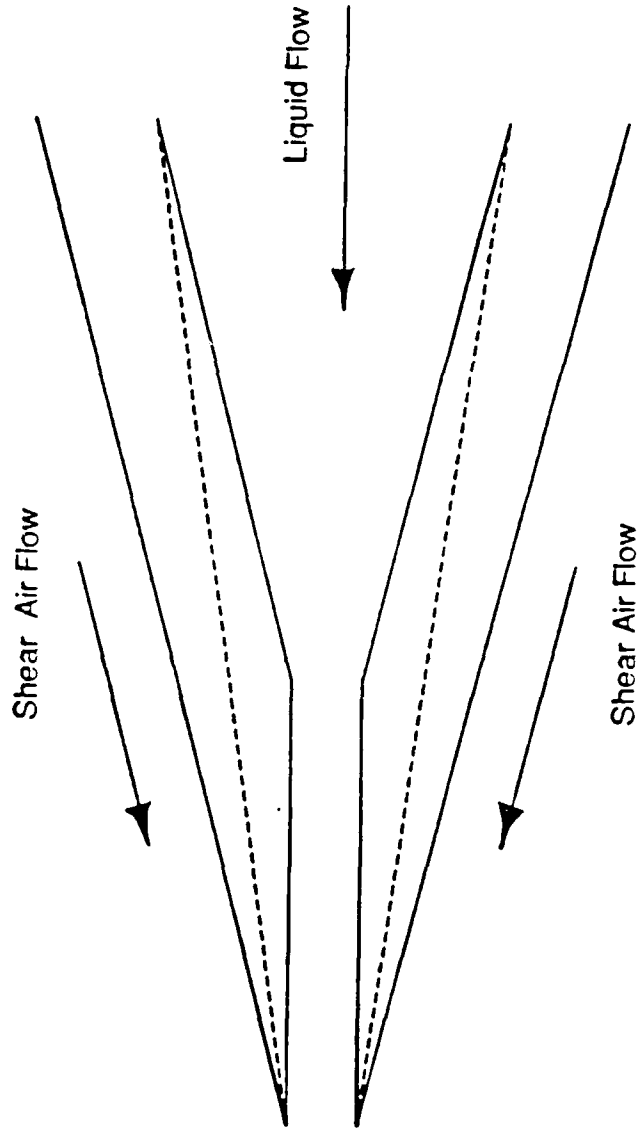
FIGURE A-3   Diagram of Prototype III Nozzle Exit Configuration with Proposed Modification.
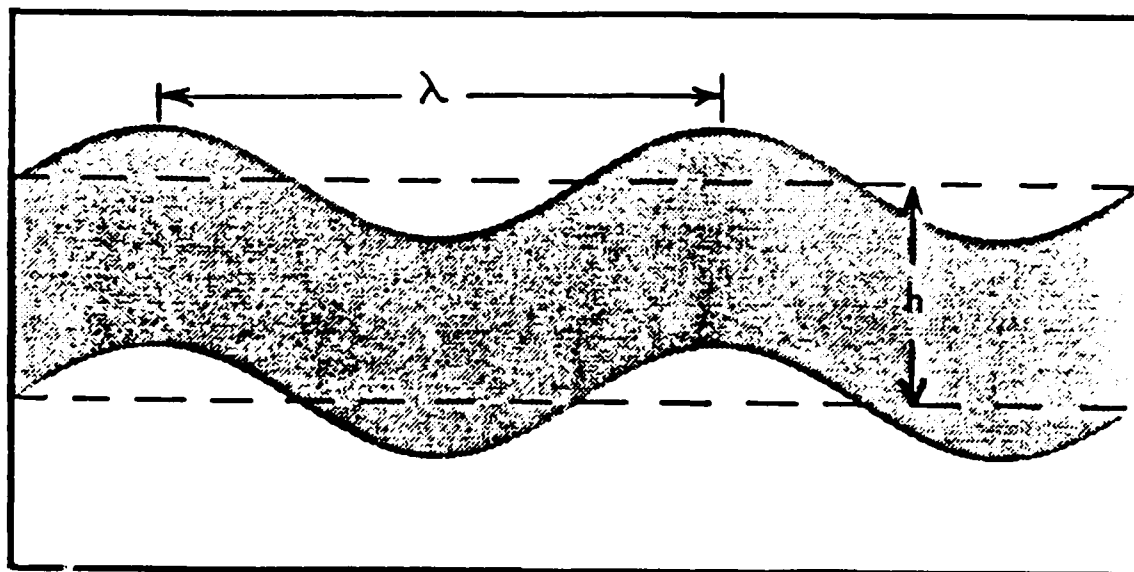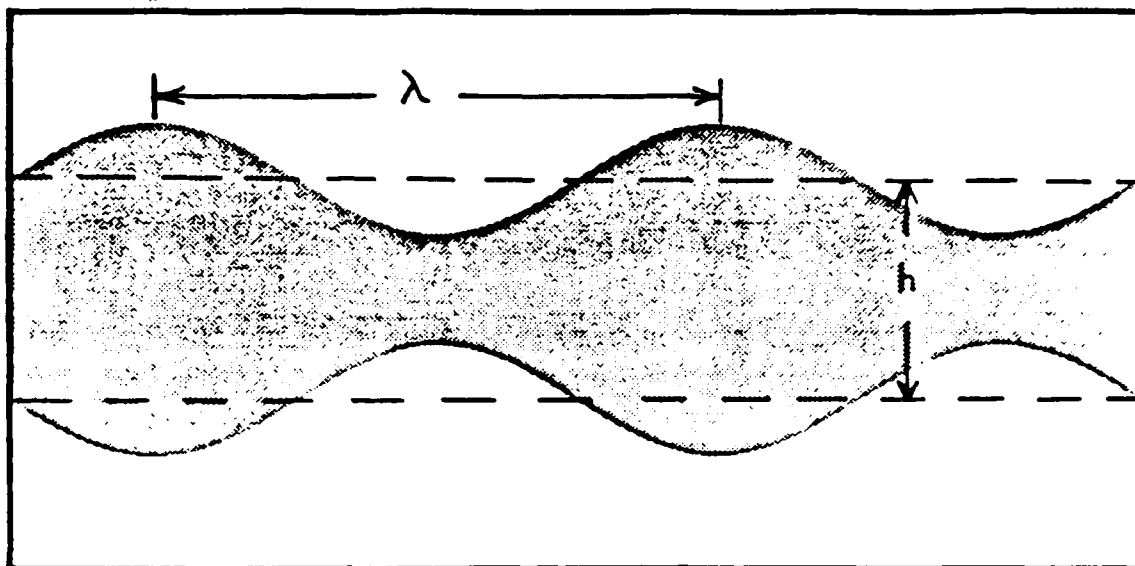
Figure B.1. Schematic of the problem of liquid sheet atomization.

2.00E+00

| t= 0.00E+00 | n = 41 | g = 1.00E+00 |

| t= 4.00E-01 | n = 41 | g = 1.00E+00 |

-2.00E+00

0.00E+00

2.00E+00

| t= 8.00E-01 | n = 44 | g = 1.00E+00 |

| t= 1.20E+00 | n = 74 | g = 1.00E+00 |

| t= 1.60E+00 | n =117 | g = 1.00E+00 |

| t= 2.00E+00 | n =165 | g = 1.00E+00 |
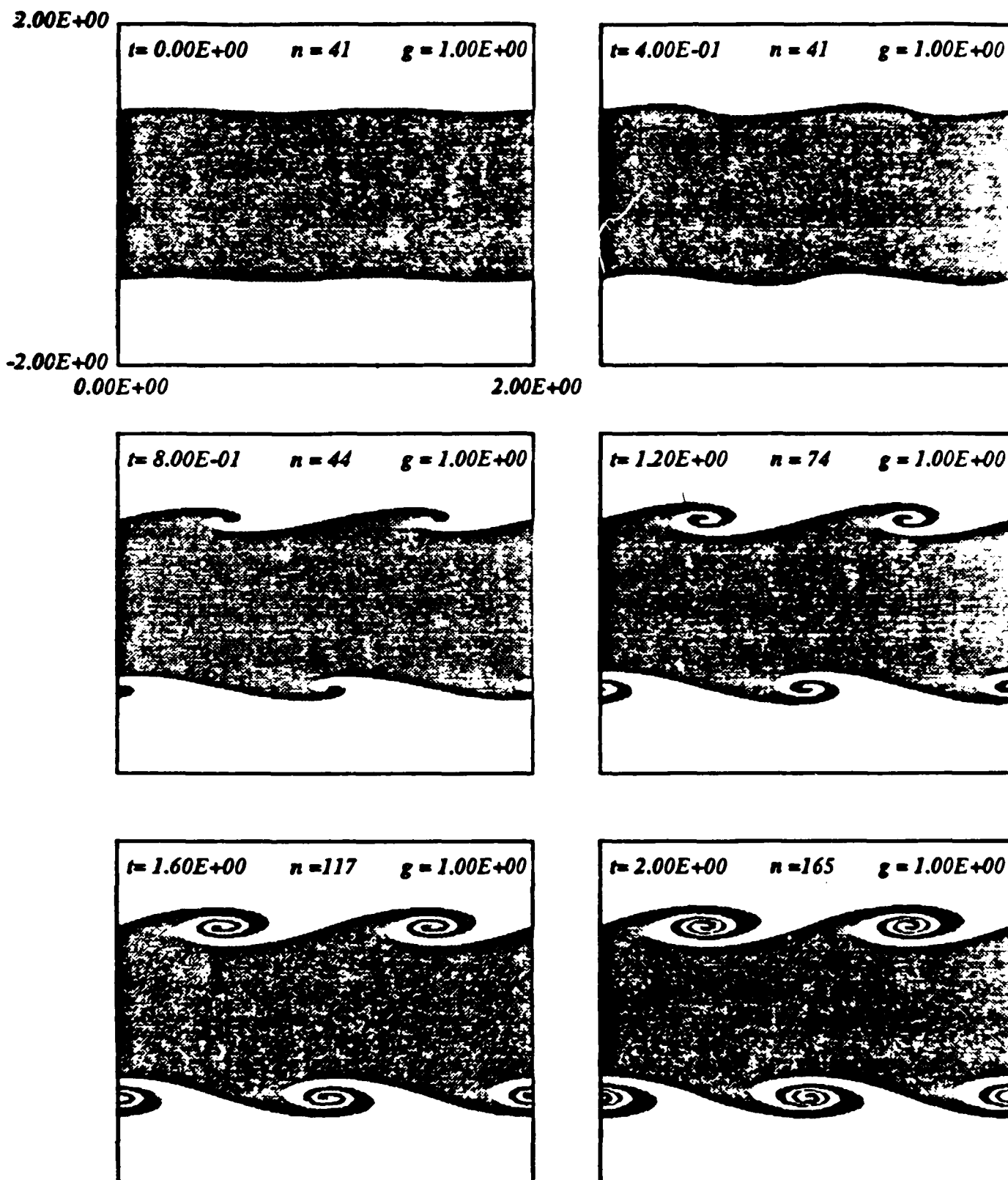
Figure B.2. Sheet evolution for a thickness-to-wavelength ratio of 2.
Density ratio=1. Surface Tension=0. (shifted-symmetric mode)
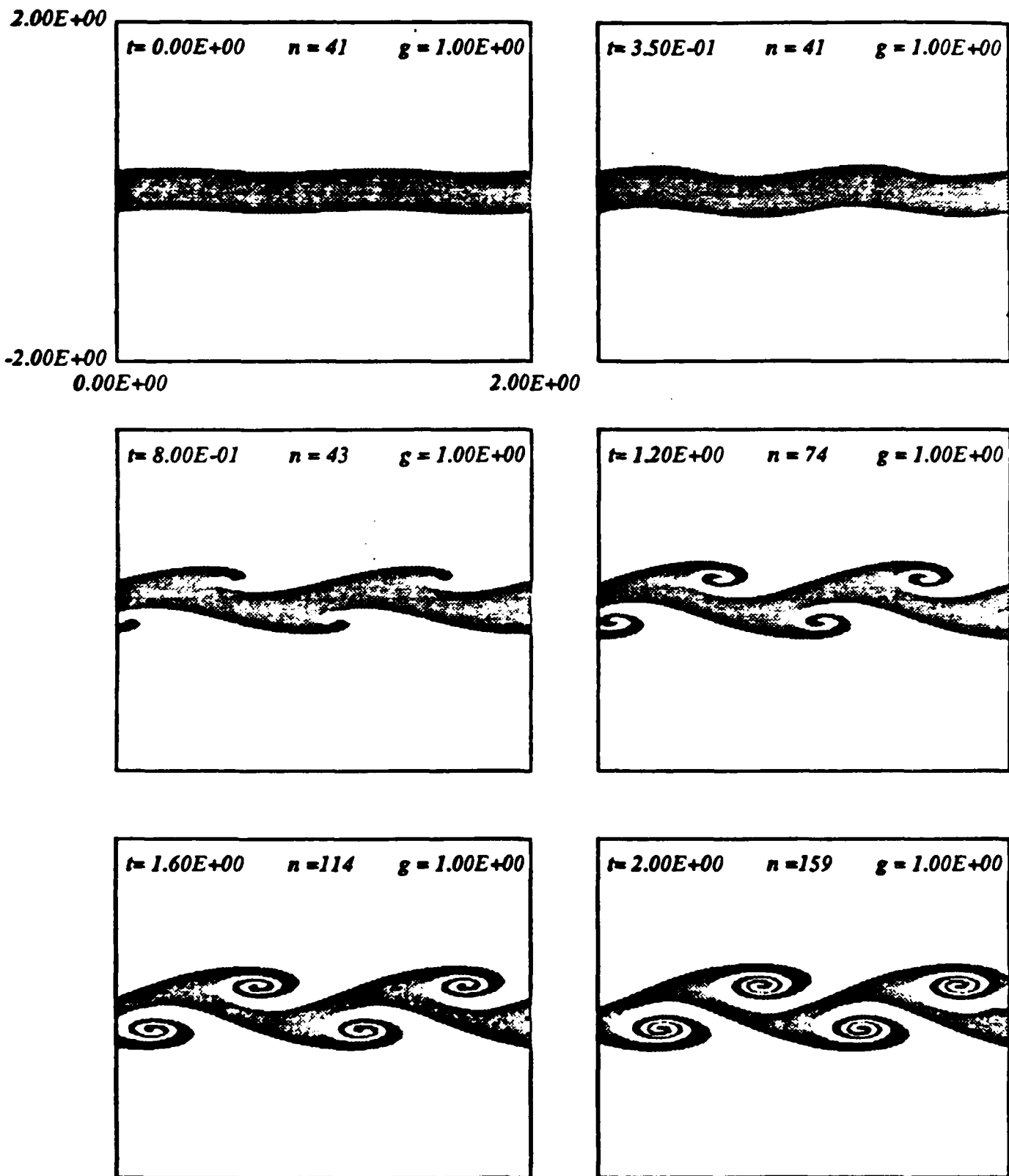
Figure B.3. Sheet evolution for a thickness-to-wavelength ratio of 1/2.
Density ratio=1. Surface Tension=0. (shifted-symmetric mode)
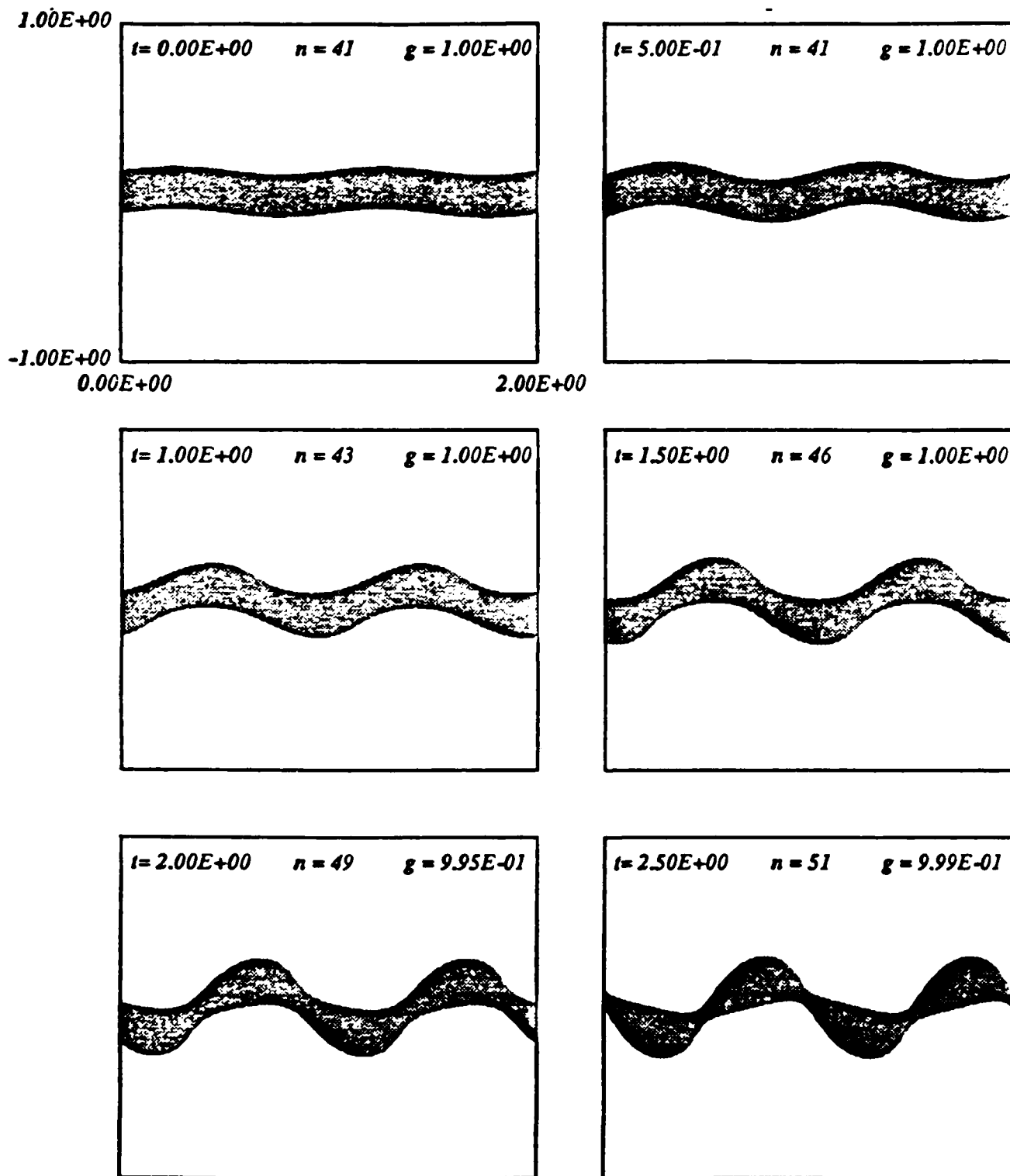
Figure B.4. Sheet evolution for a thickness-to-wavelength ratio of 1/4.
Density ratio=1. Optimum dimensionless wavenumber. (shifted-symmetric mode)
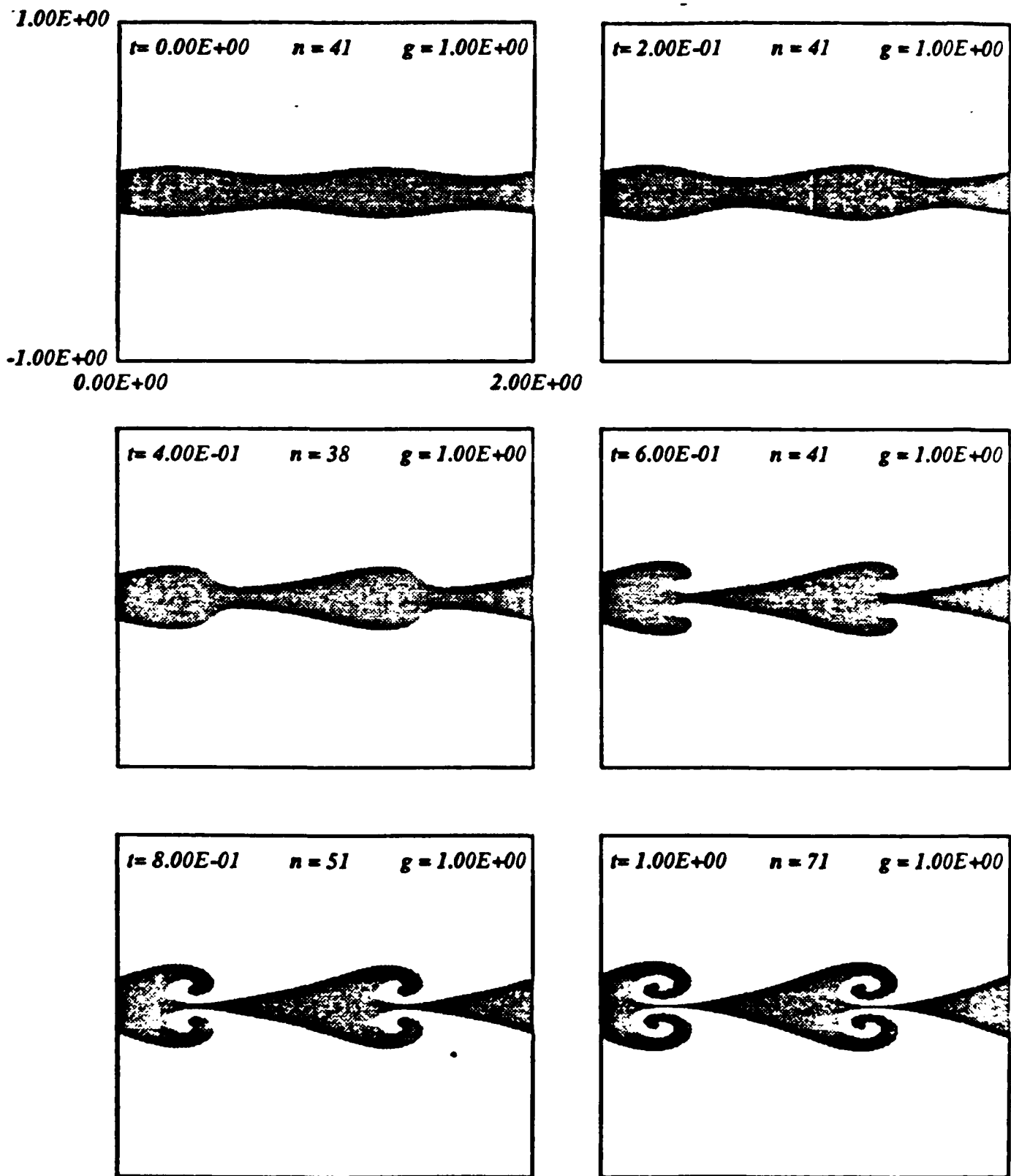
Figure B.5. Sheet evolution for a thickness-to-wavelength ratio of 1/4.
Density ratio=1. No surface tension. (symmetric mode)
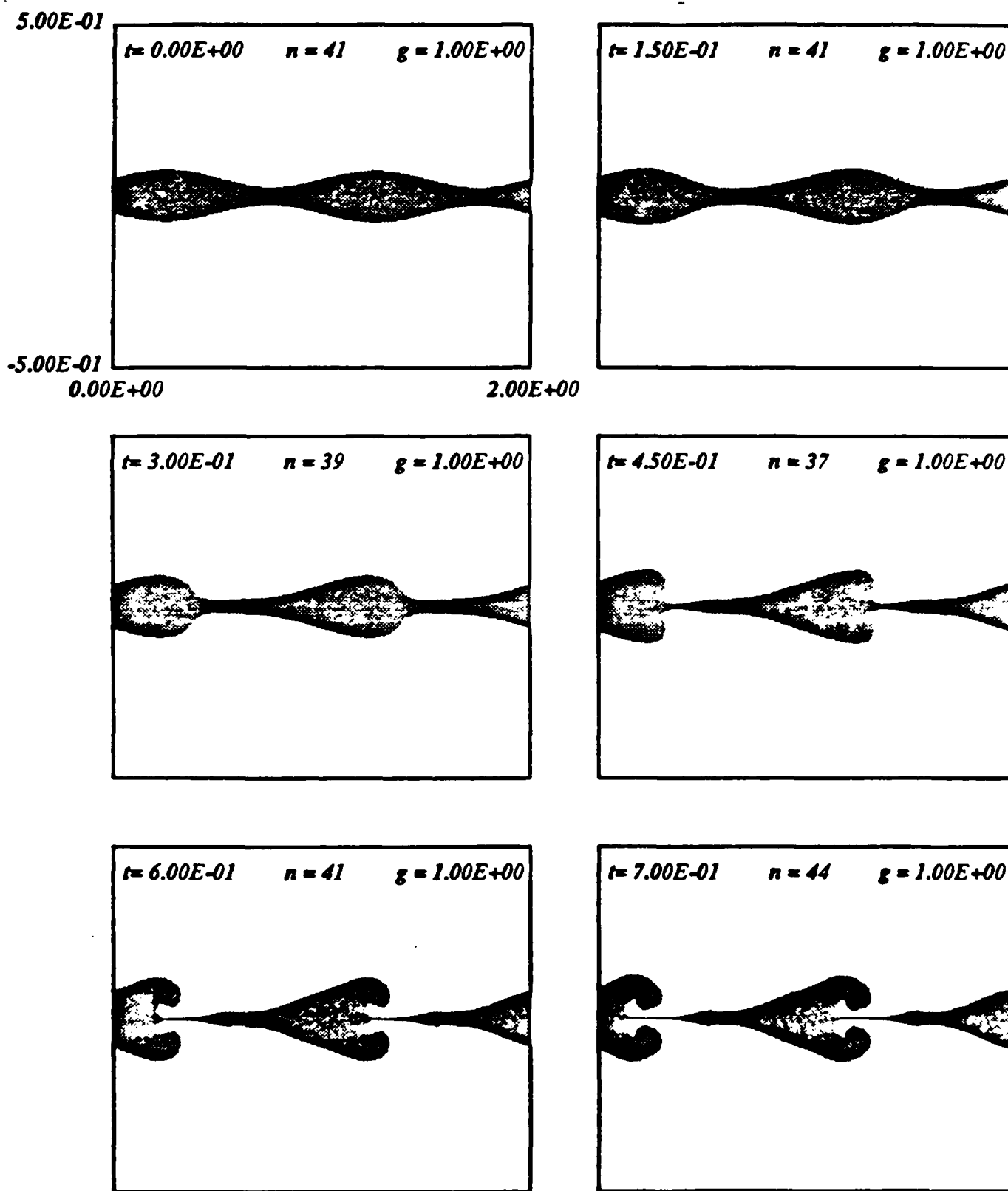
Figure B.6. Sheet evolution for a thickness-to-wavelength ratio of 1/8.
Density ratio=1. No surface tension. (symmetric mode)
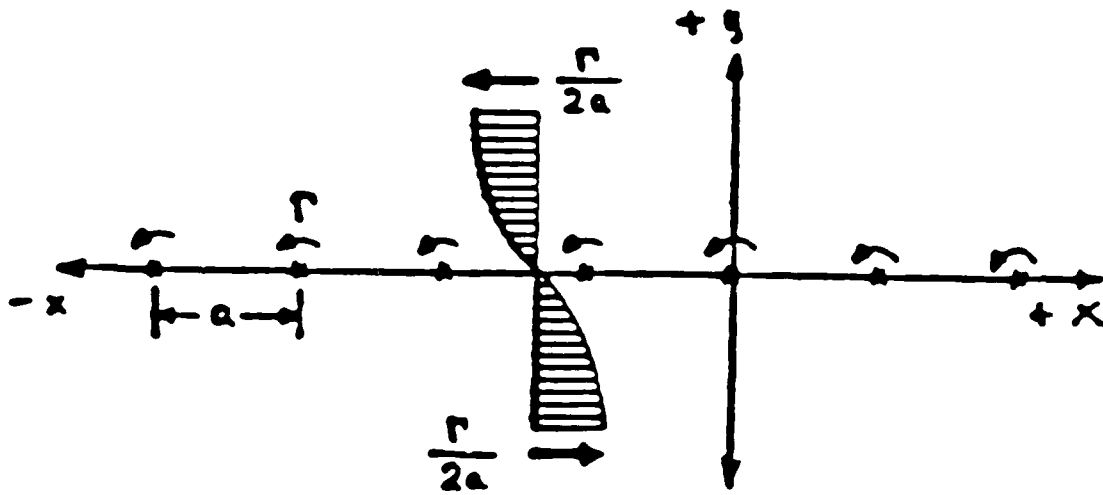
Fig. C.1. Schematic of the problem.
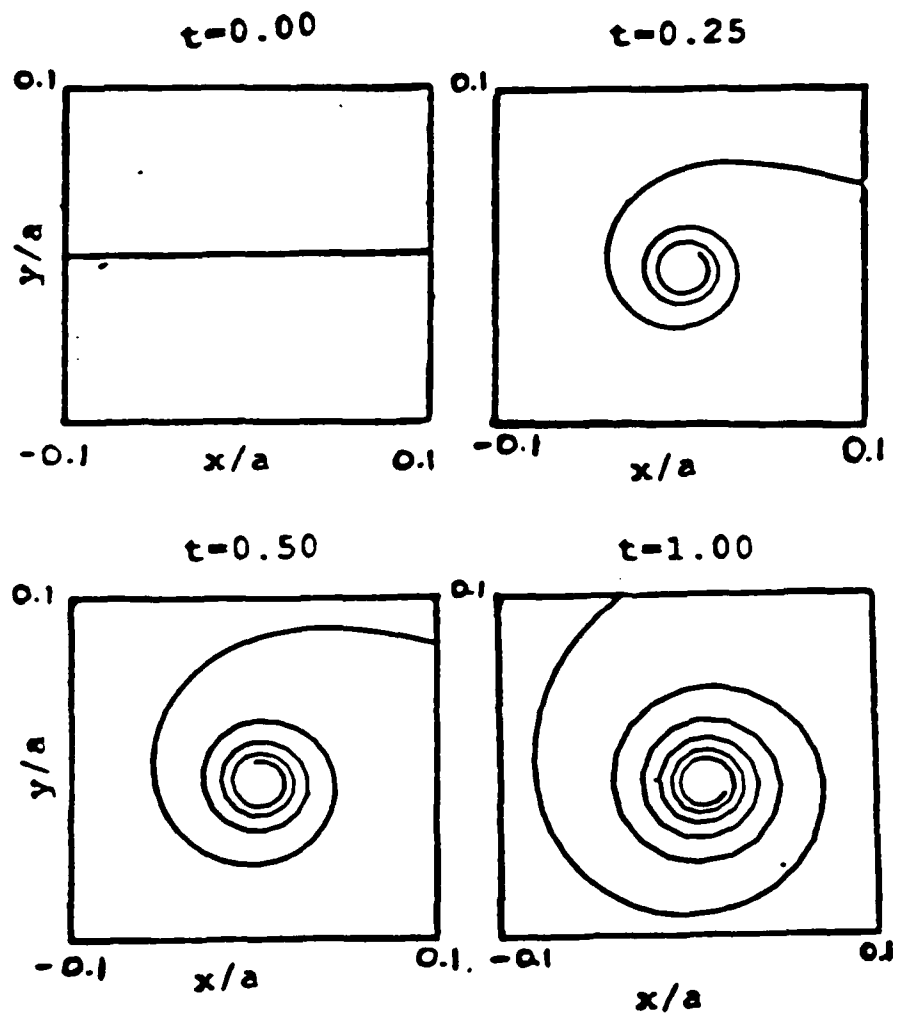
Fig. C.2. Evolution of the interface for Re=50.
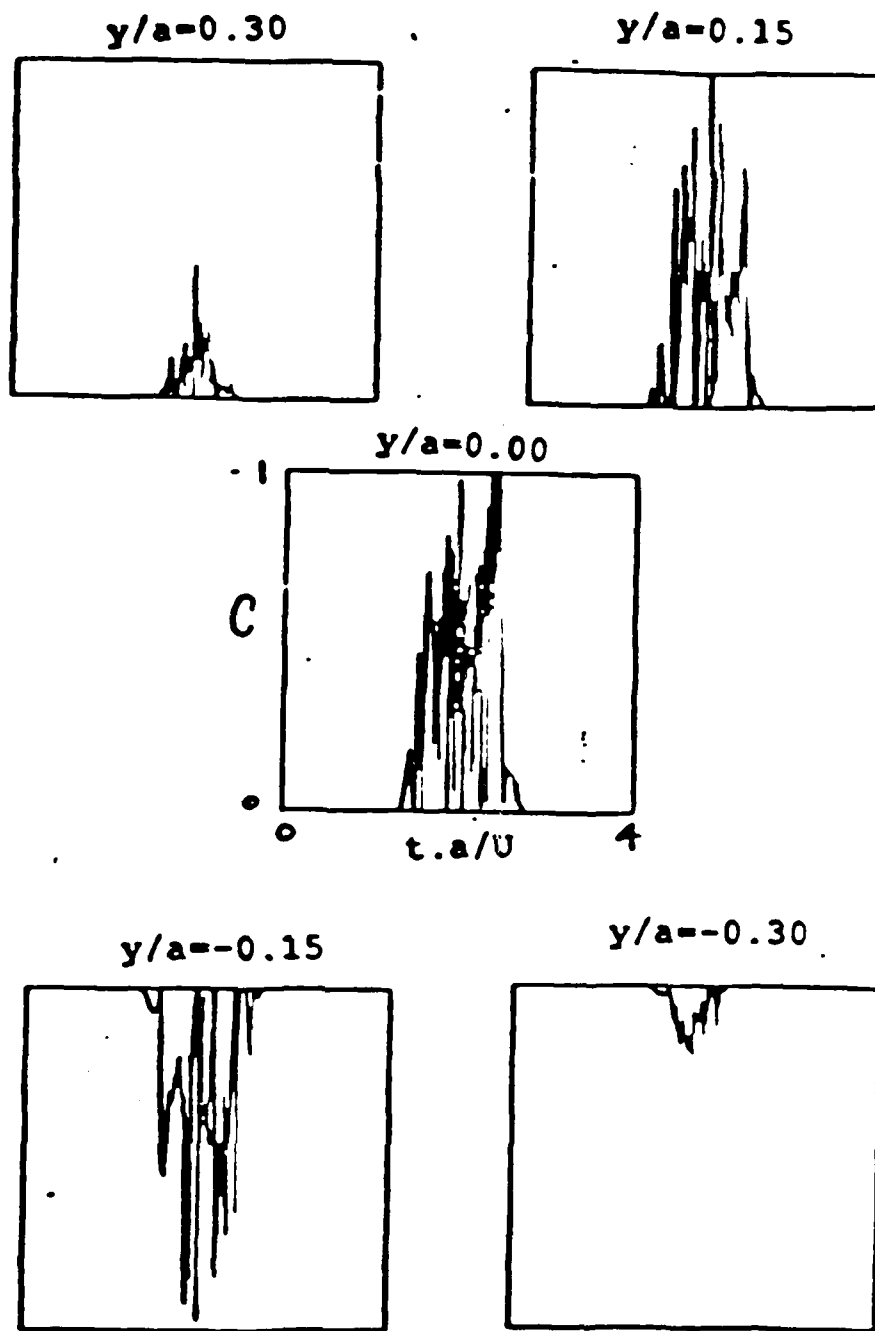
Fig. C.3. Concentration Profiles for Re=50, Sc=1.
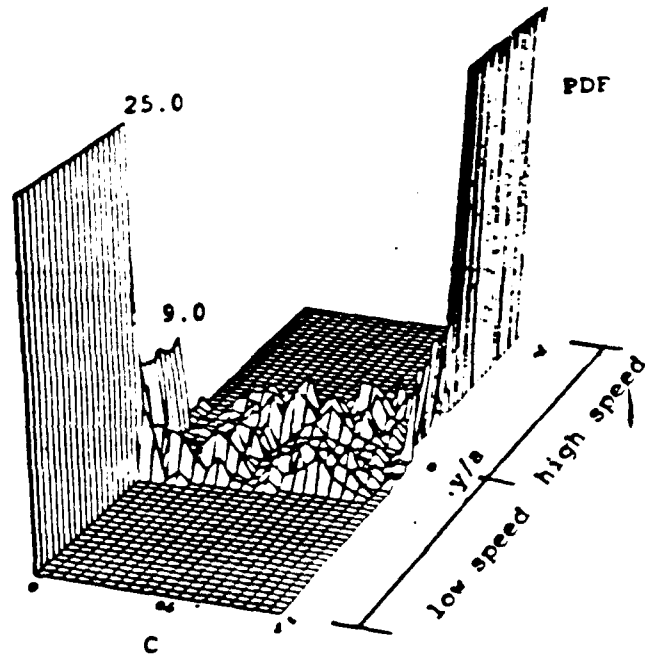
Fig. C.4a Species Concentration PDF for Re=50, Sc=1.
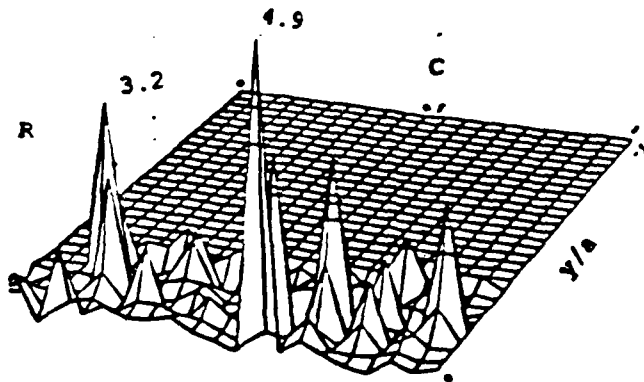
Fig. C.4b Relative difference between PDF on high low speed sides.
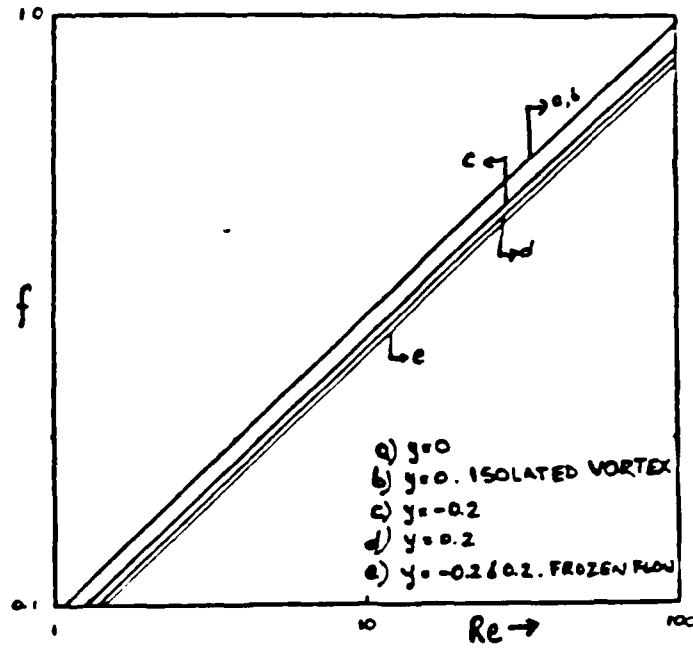
Fig. C.5a   Mixedness parameter as a function of Re and
height above the mixing plane.
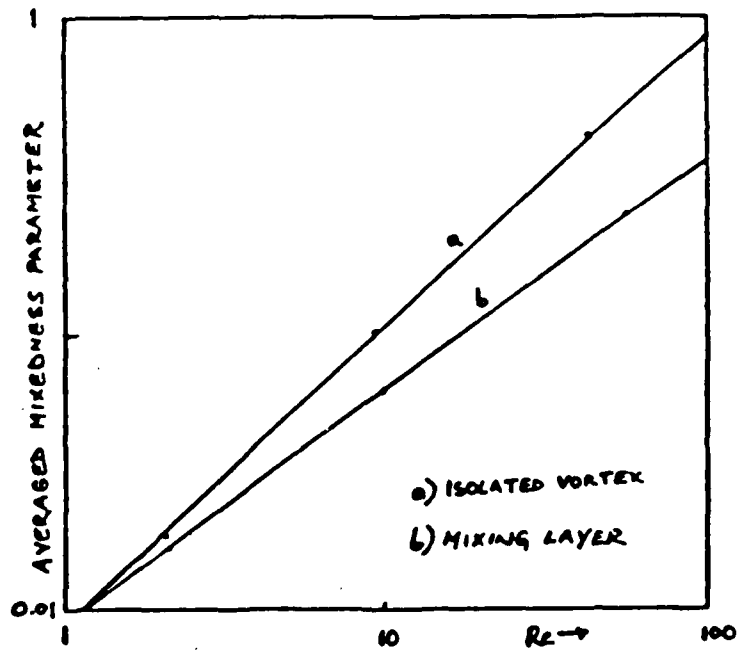
Fig. C.5b   Comparison between the mixedness for an isolated
vortex and a mixing layer.
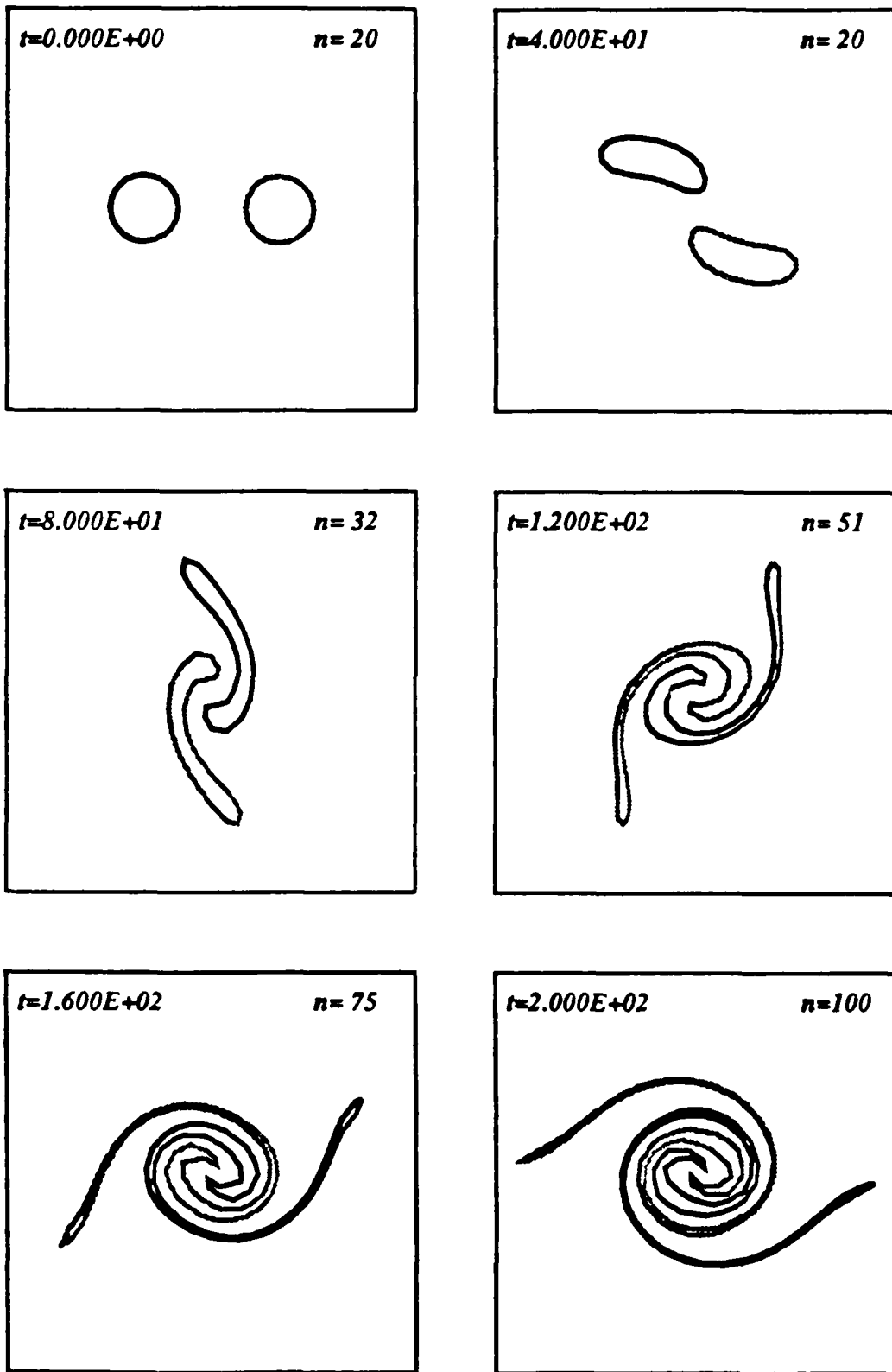
Figure C.6. The interaction of two vortex tubes whose centers
are initially two diameters apart
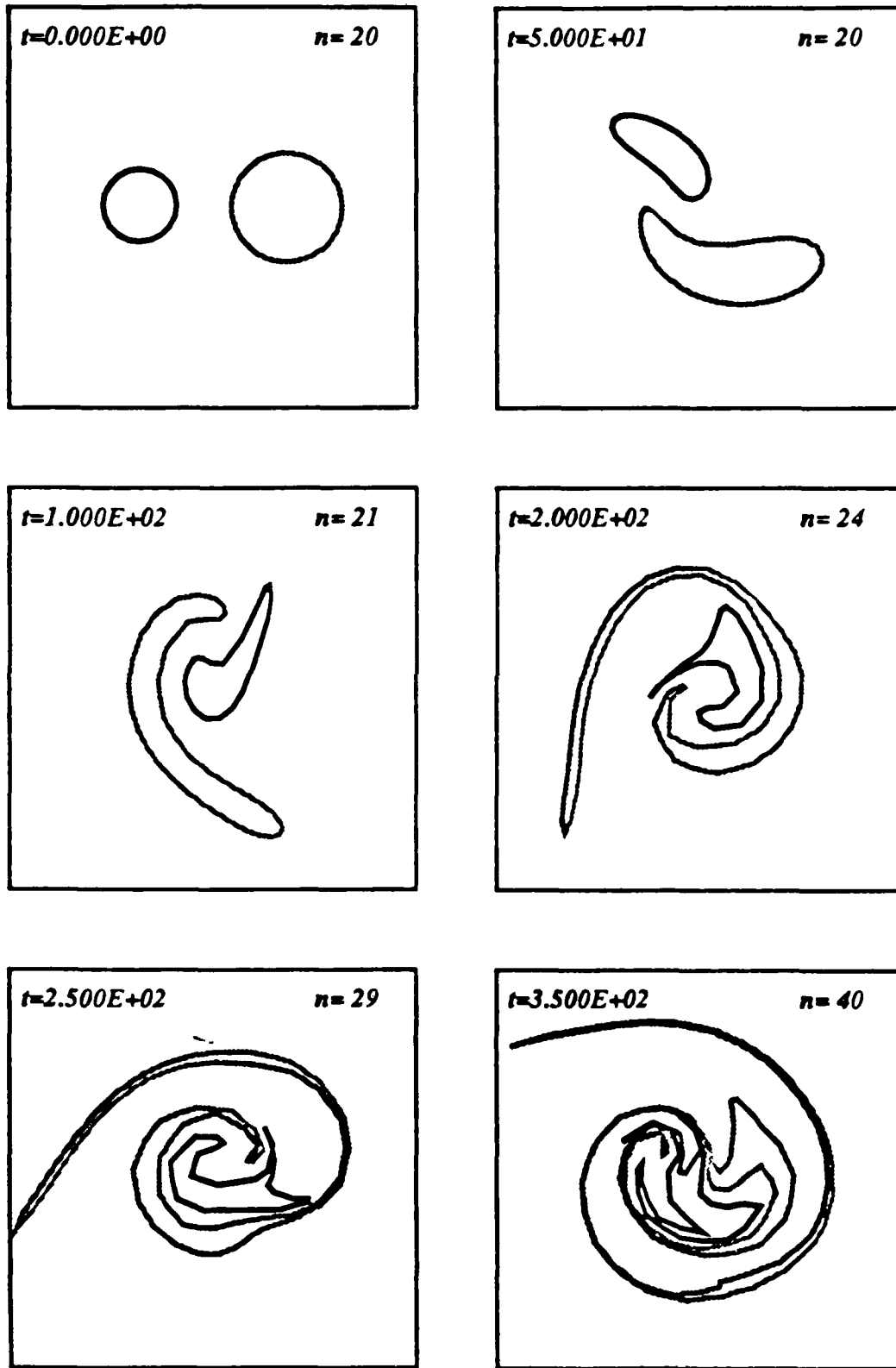
Figure C.7. The interaction of two vortex tubes with a size ratio of 2/3.
The centers are initially four small diameters apart
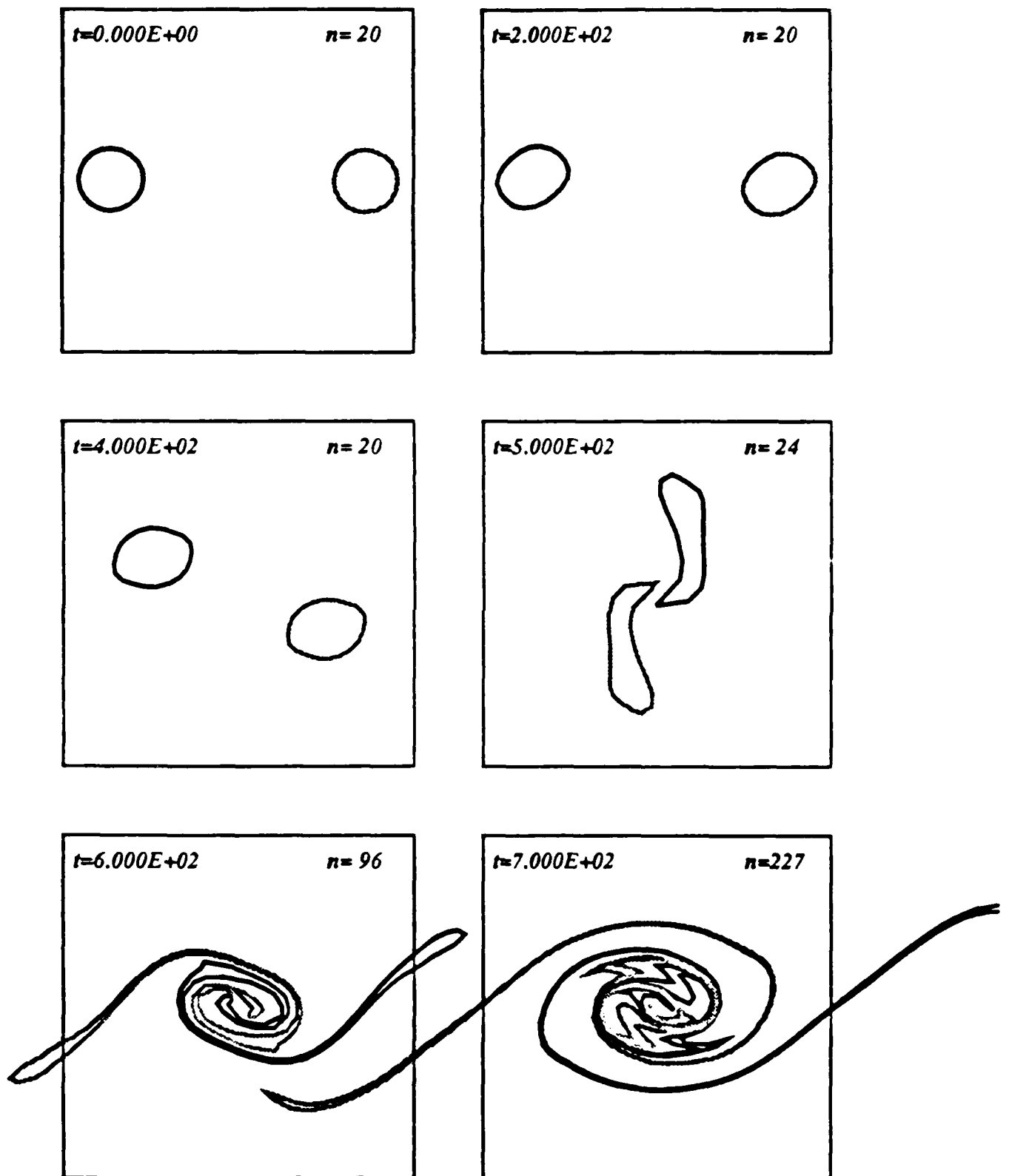
Figure C.8. The interaction of two vortex tubes whose centers are initially four diameters apart in the presence of an infinite row of point vortices.
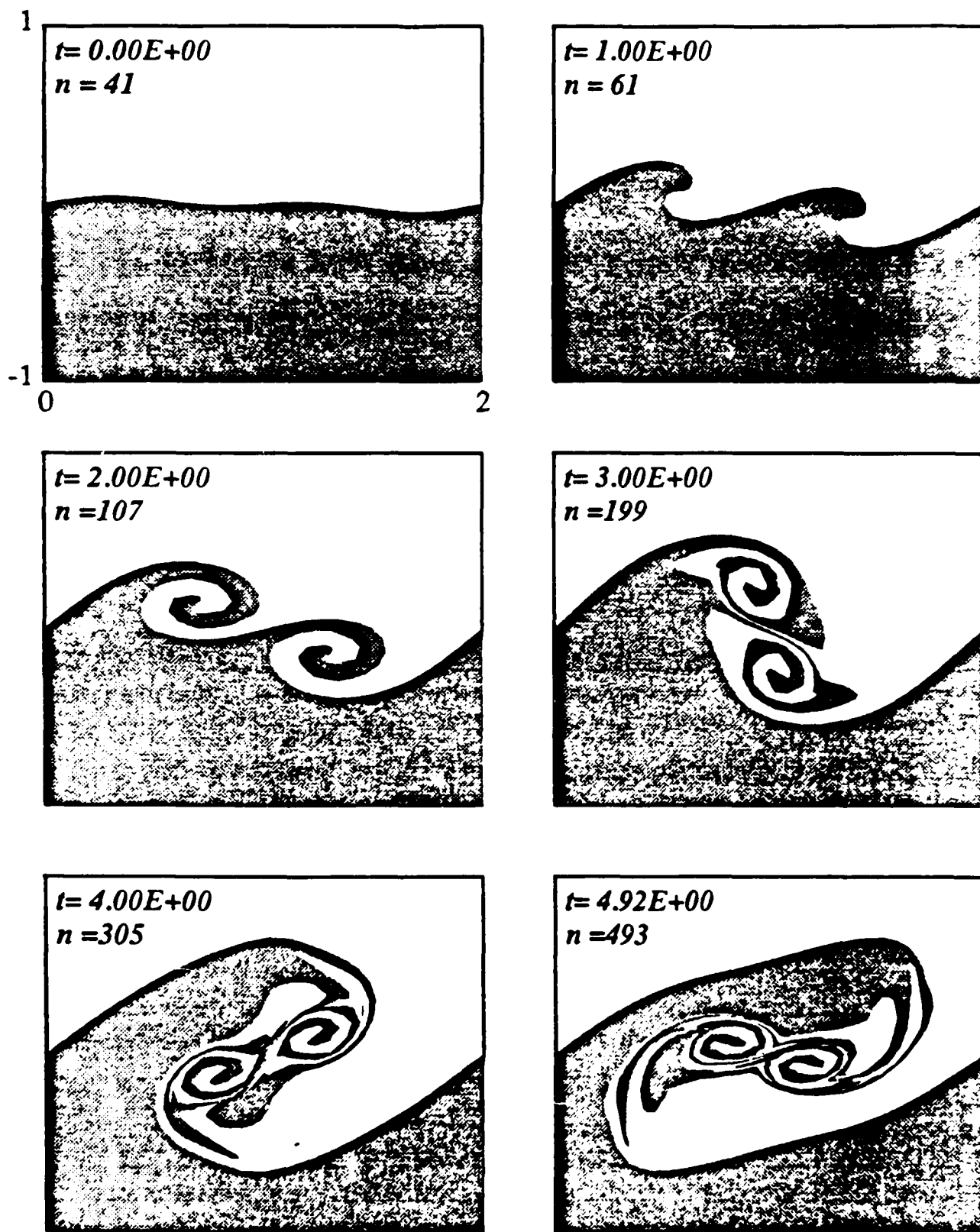
Figure C.9. Rollup and pairing of two vortical structures induced by the presence of the first subharmonic.
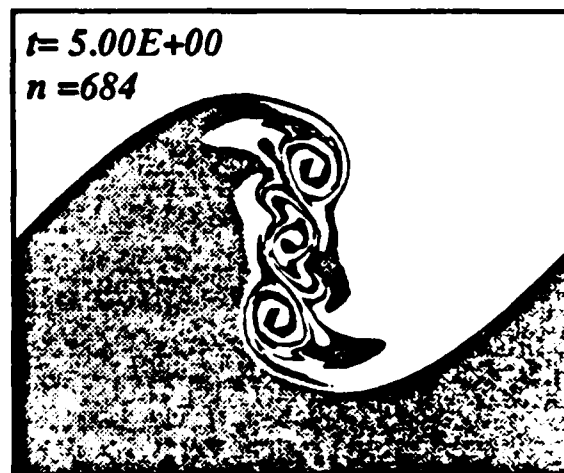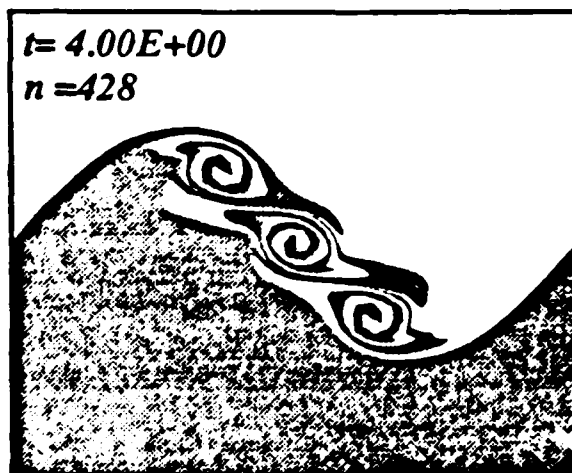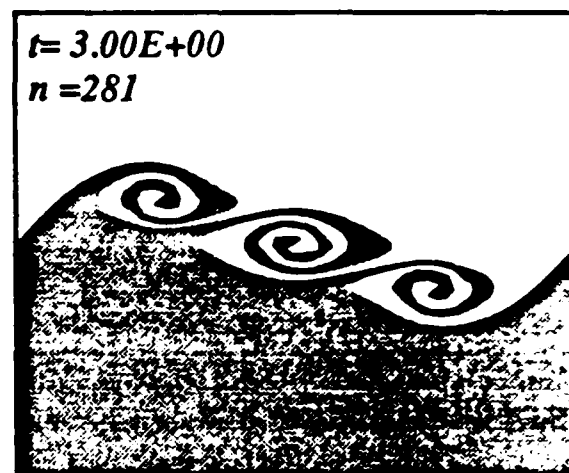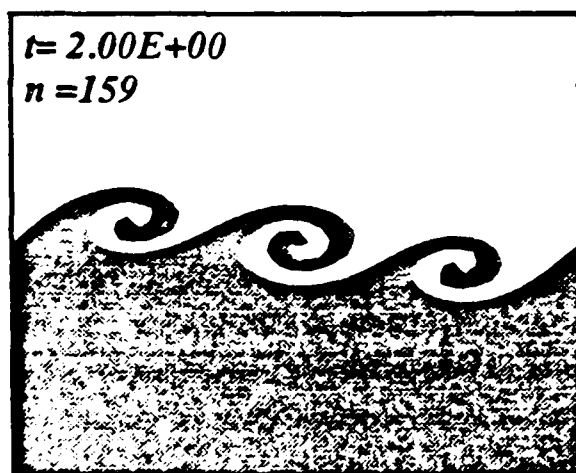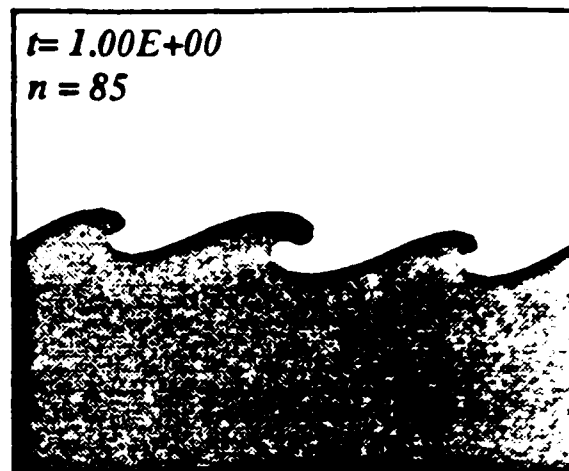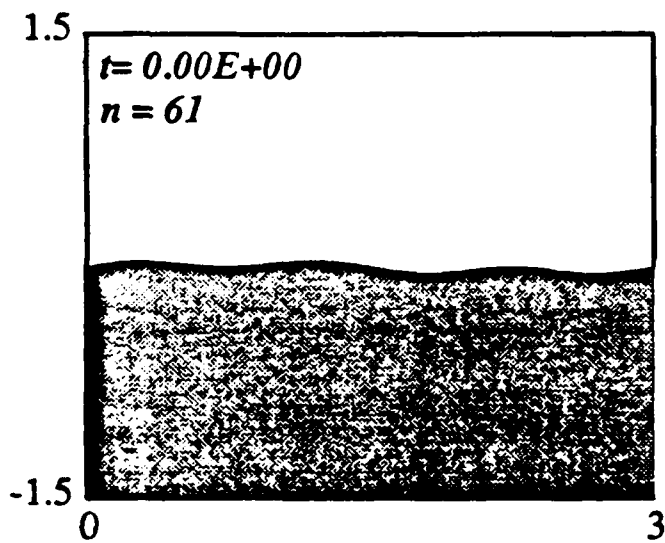
Figure C.10. Rollup and grouping of three vortical structures
induced by the presence of the second subharmonic.
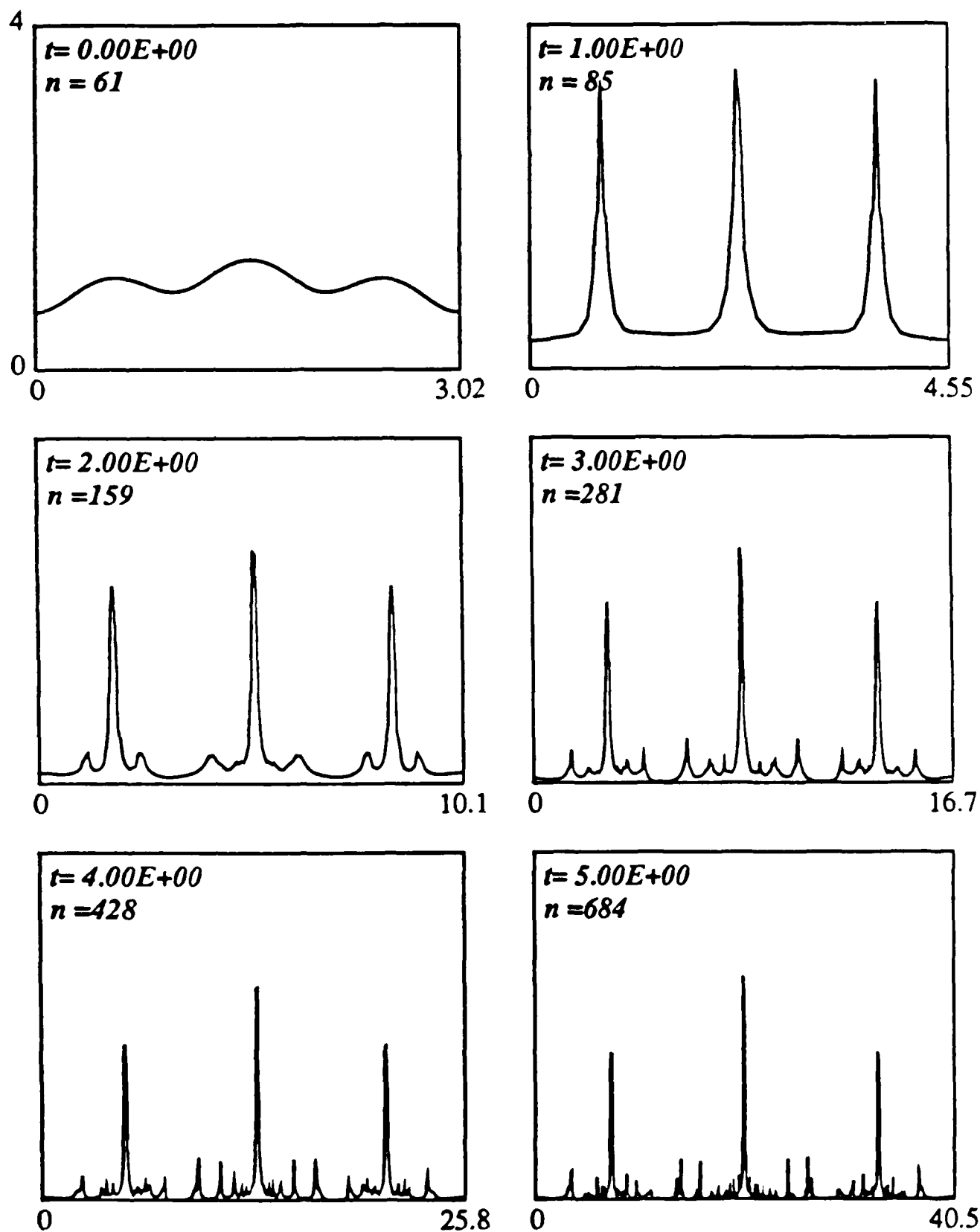
Figure C.11. Evolution of the vorticity distribution along the interface during the grouping of three vortical structures.
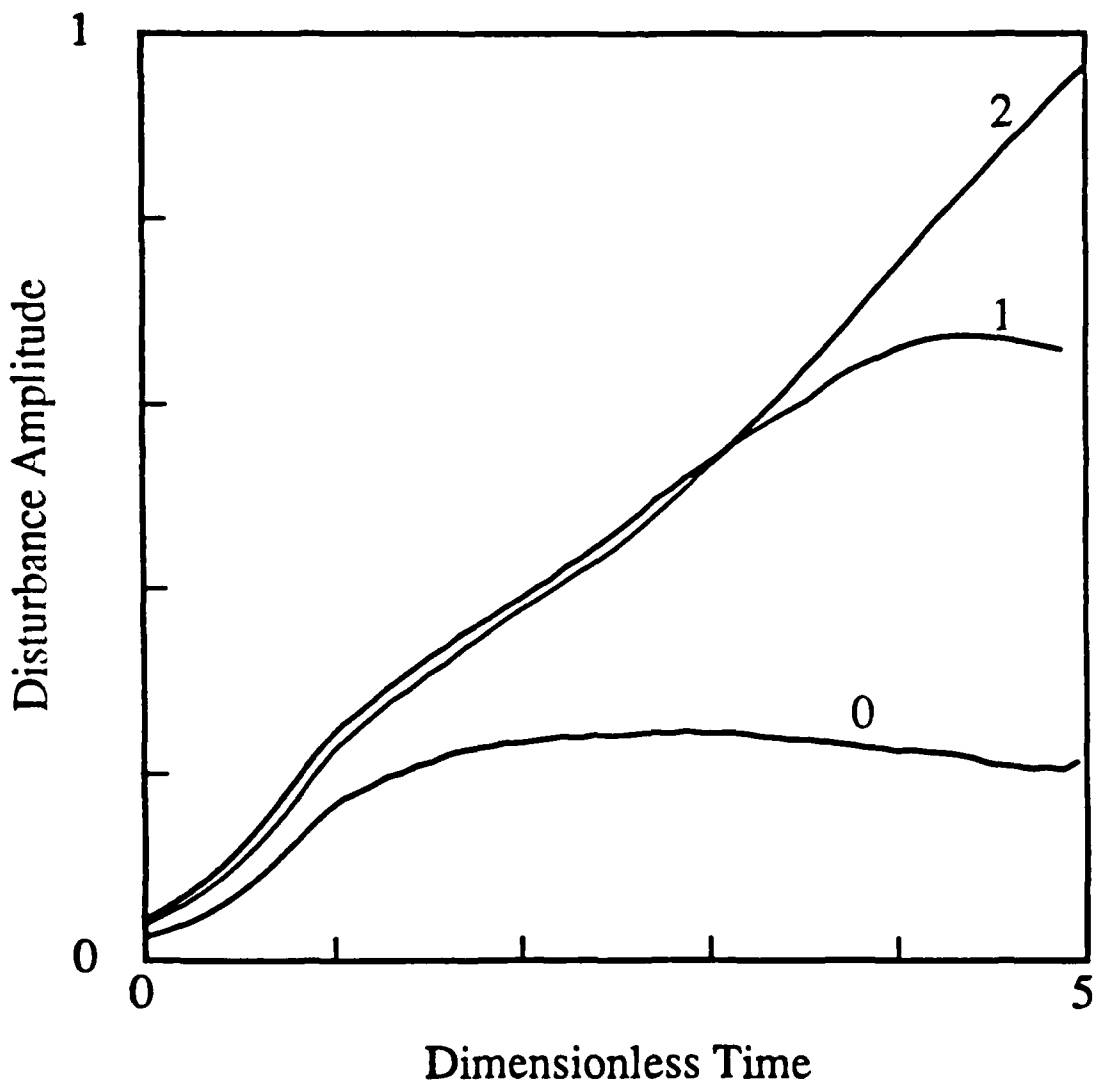
Figure C.12. Amplitude of the disturbance as a function of time for
the fundamental disturbance alone (0), the fundamental plus the first
subharmonic (1), and the fundamental plus the second subharmonic (2).

(a)
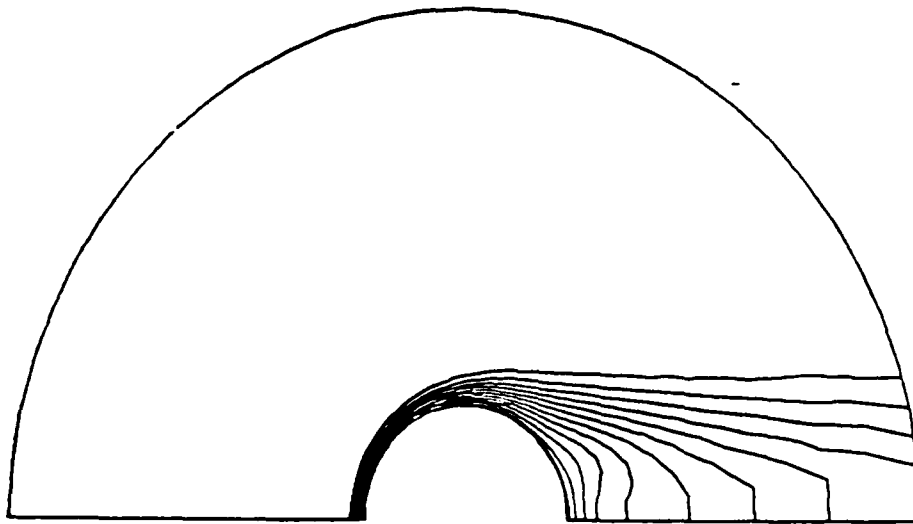
MASS FRACTION
TIME = 5.000
GAS PHASE REYNOLDS NUMBER = 62.117
AMBIENT TEMPERATURE = 800 Degree Kelvin
INITIAL DROPLET TEMPERATURE = 300 Degree Kelvin

(b)

761.78
723.41
685.11

508.52   414.54
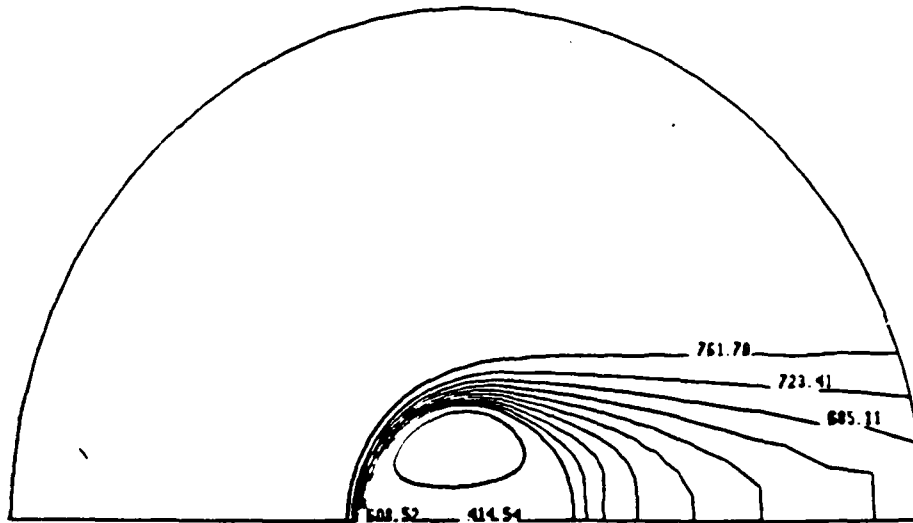
GAS AND LIQUID PHASE ISOTHERMS
TIME = 5.000
GAS PHASE REYNOLDS NUMBER = 62.117
AMBIENT TEMPERATURE = 800 Degree Kelvin
INITIAL DROPLET TEMPERATURE = 300 Degree Kelvin

Figure D.1. Contour plots: (a) mass fraction, (b) temperature of liquid and
gas phases, (c) stream function of liquid phase, (d) isotherms of
liquid phase, (e) vorticity, (f) instantaneous velocity of gas
phase.

(c)
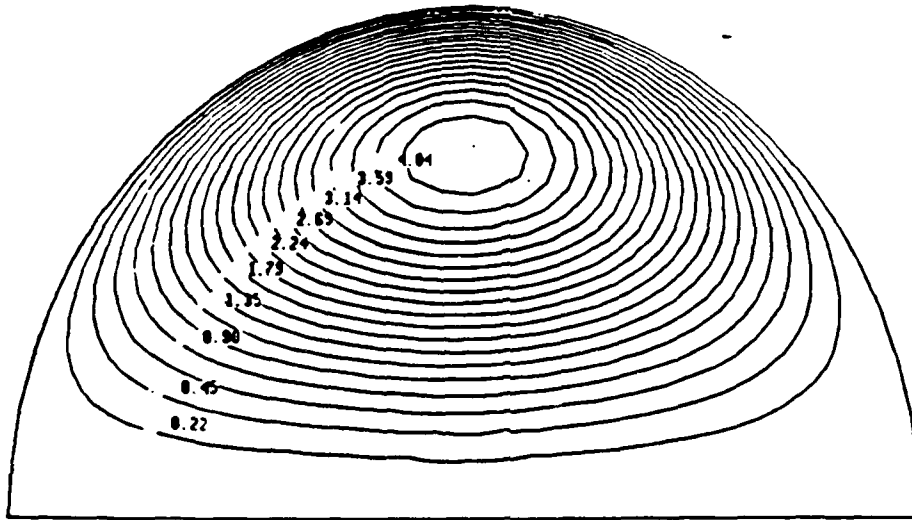
LIQUID PHASE STREAM FUNCTION
TIME = 5.000
GAS PHASE REYNOLDS NUMBER = 52.117
AMBIENT TEMPERATURE = 800 Degree Kelvin
INITIAL DROPLET TEMPERATURE = 300 Degree Kelvin

(d)
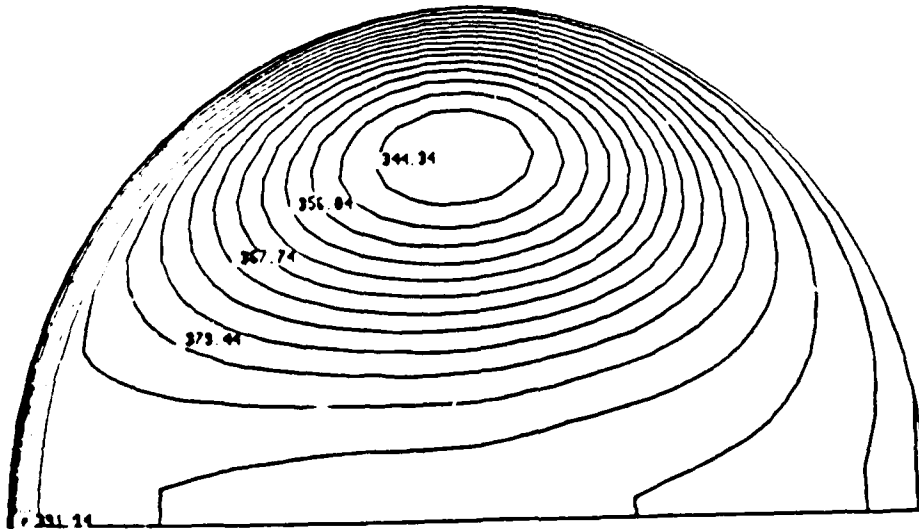
LIQUID PHASE ISOTHERMS
TIME = 5.000
GAS PHASE REYNOLDS NUMBER = 52.117
AMBIENT TEMPERATURE = 800 Degree Kelvin
INITIAL DROPLET TEMPERATURE = 300 Degree Kelvin

(e)
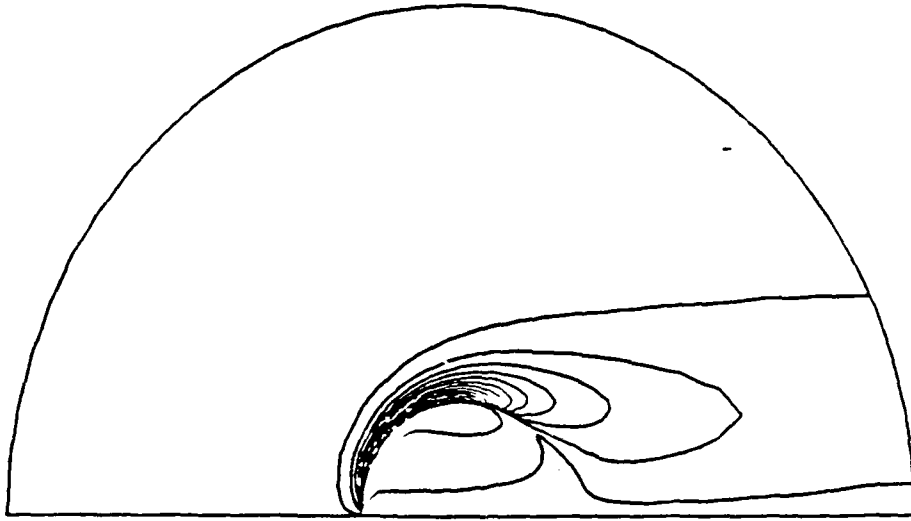
GAS AND LIQUID PHASE VORTICITY
TIME = 5.000
GAS PHASE REYNOLDS NUMBER = 62.117
AMBIENT TEMPERATURE = 500 Degree Kelvin
INITIAL DROPLET TEMPERATURE = 300 Degree Kelvin

TWO DIMENSIONAL ADVANCED DROPLET MODEL

VARIABLE PHYSICAL PROPERTIES

(f)
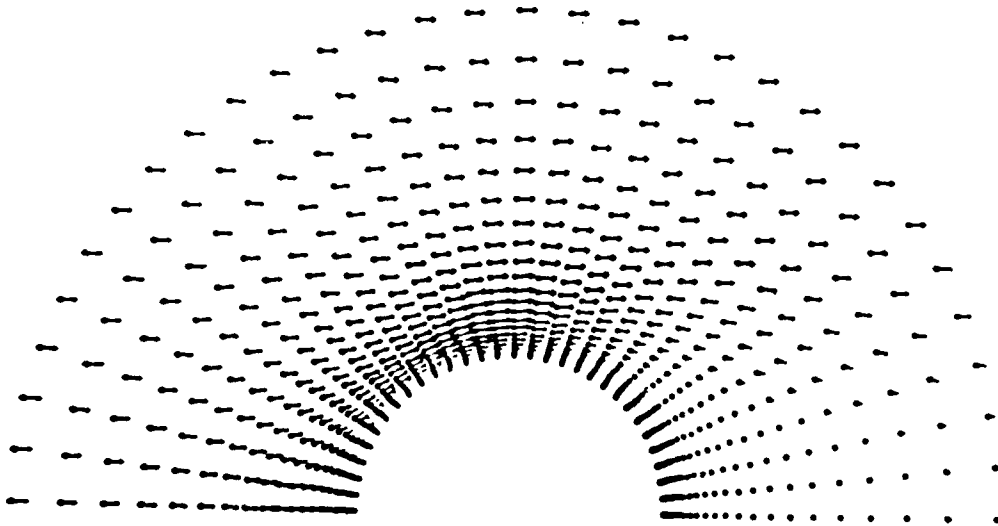
GAS PHASE VELOCITY FIELD
HYDRODYNAMIC DIFFUSION TIME = 1.000
GAS PHASE REYNOLDS NUMBER = 69.375
AMBIENT TEMPERATURE = 500 Degree Kelvin
INITIAL DROPLET TEMPERATURE = 300 Degree Kelvin
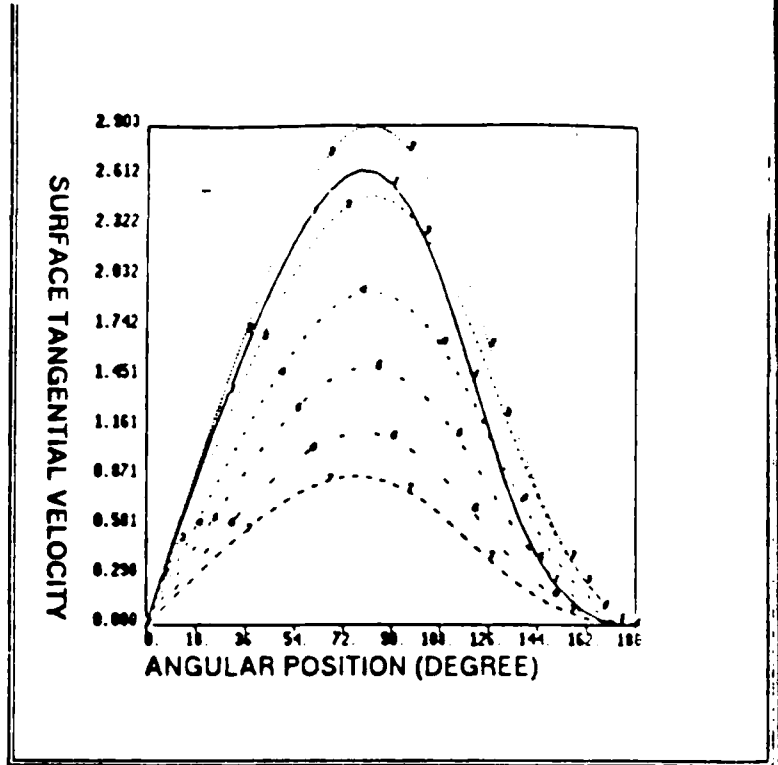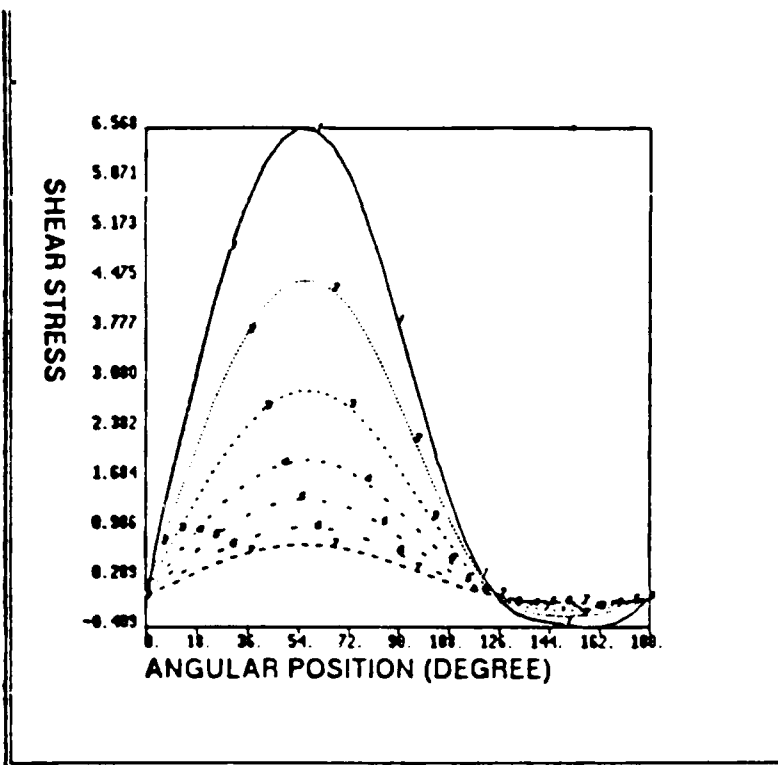
Figure D.2. (a) Surface shear stress distribution, (b) surface tangential velocity distribution at different times, 1 - time = 0.98, Re = 91.30; 2 - time = 3.00, Re = 93.83; 3 - time = 5.63, Re = 59.02; 4 - time = 8.30, Re = 49.21; 5 - time = 11.25, Re = 38.61; 6 - time = 14.38, Re = 30.96; 9 - time = 19.13, Re = 25.63.
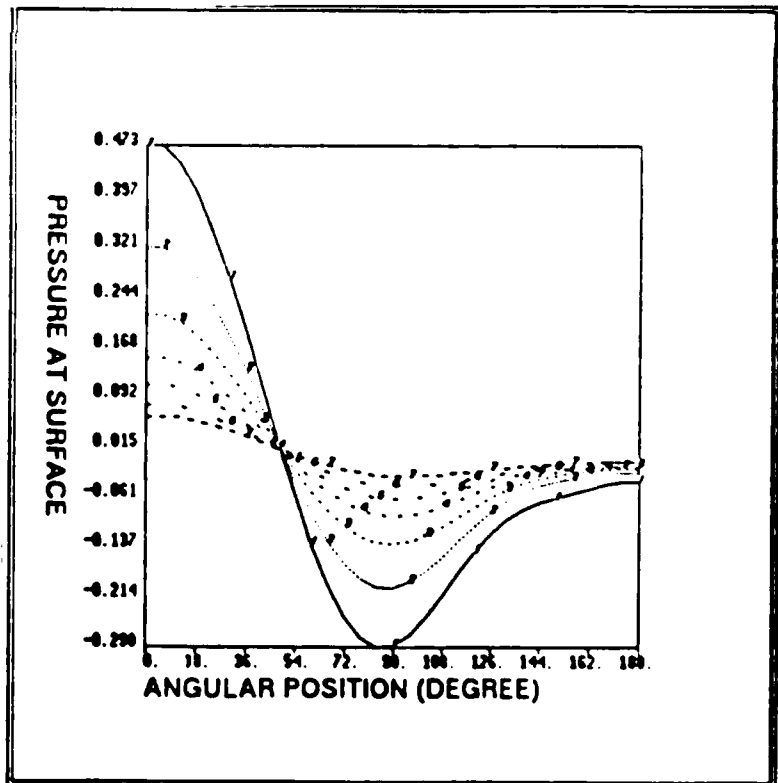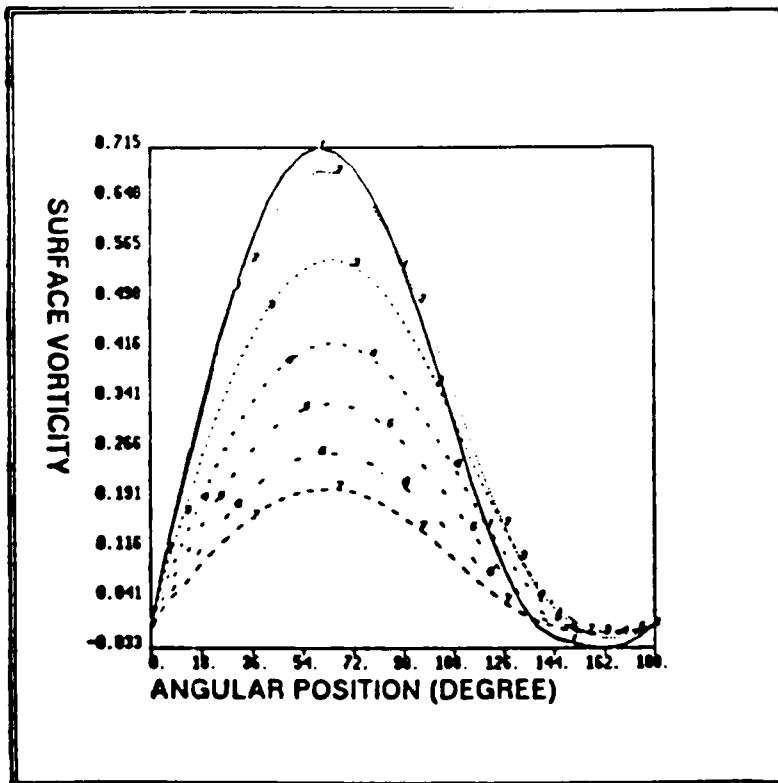
Figure D.2. (c) Surface vorticity distribution, (d) surface nondimensional pressure distribution at different times, 1 - time = 0.98, Re = 91.30; 2 - time = 3.00, Re = 93.83; 3 - time = 5.63, Re = 59.02; 4 - time = 8.30, Re = 49.21; 5 - time = 11.25, Re = 38.61; 6 - time = 14.38, Re = 30.96; 9 - time = 19.13, Re = 25.63.
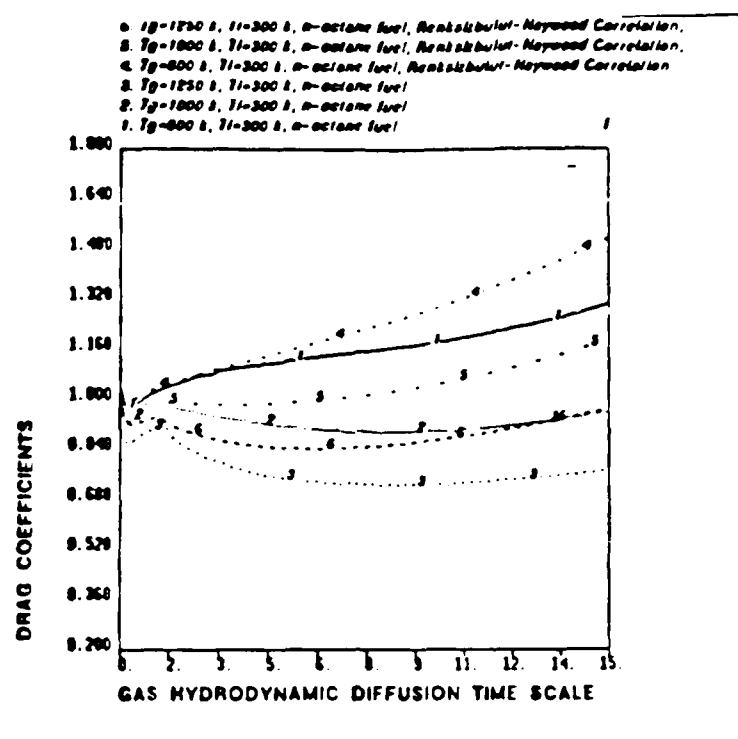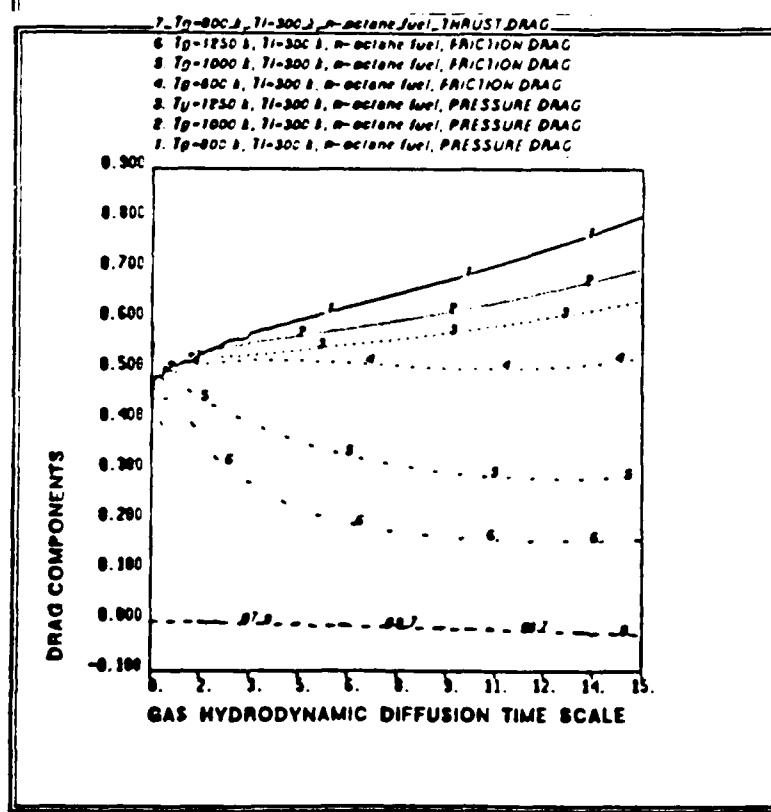
Figure D.3. (a) Time variation of drag coefficients for different ambient temperatures, (b) time variation of three drag components for different ambient temperatures.
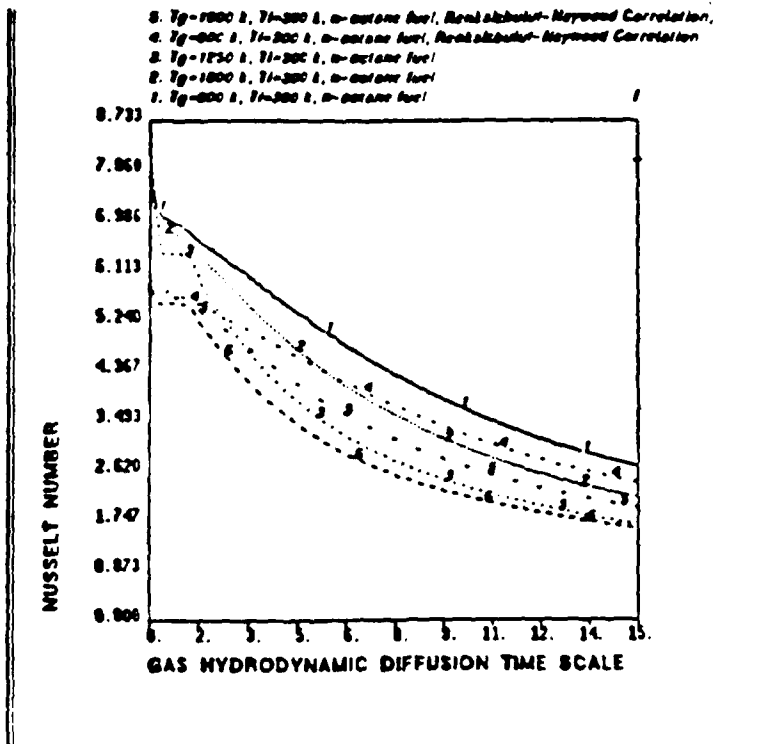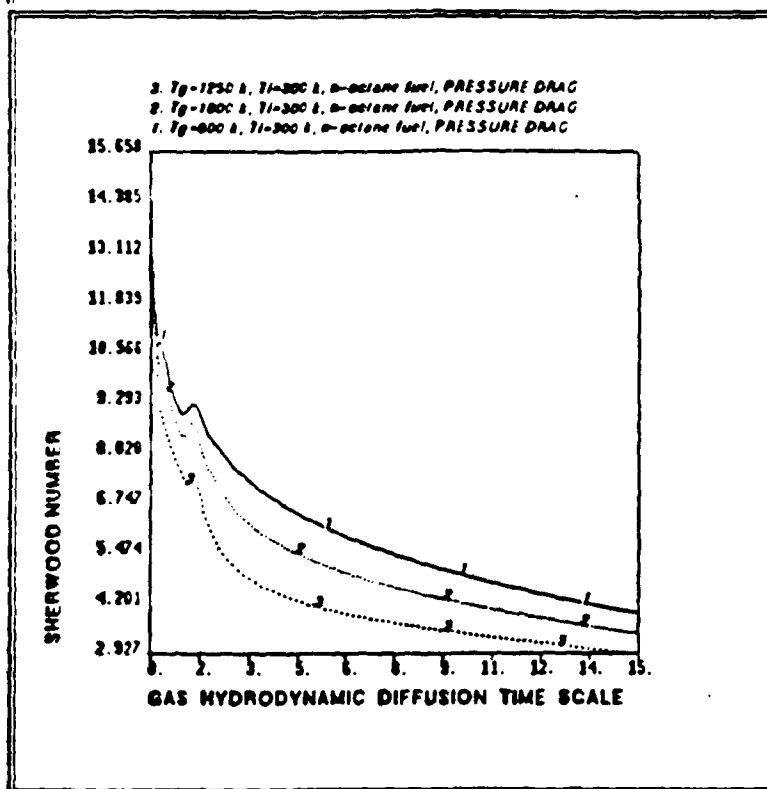
Figure D.4. (a) Time variation of average Nusselt numbers for different ambient temperatures, (b) time variation of average Sherwood numbers for different ambient temperatures.

(a)
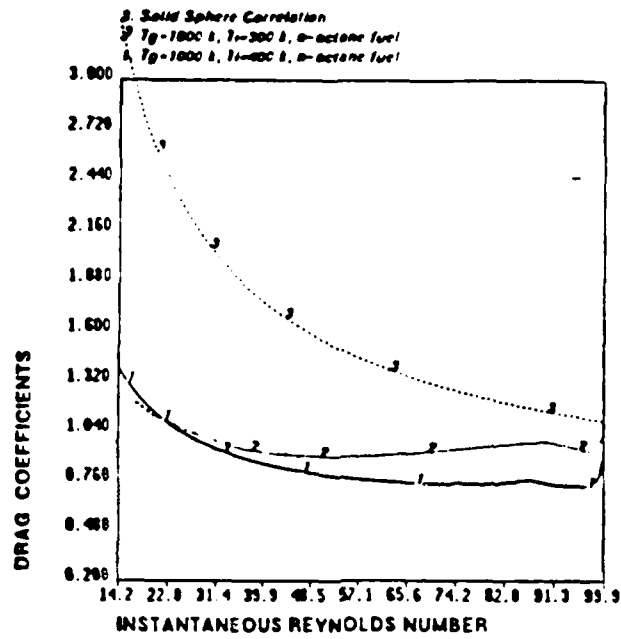
(b)
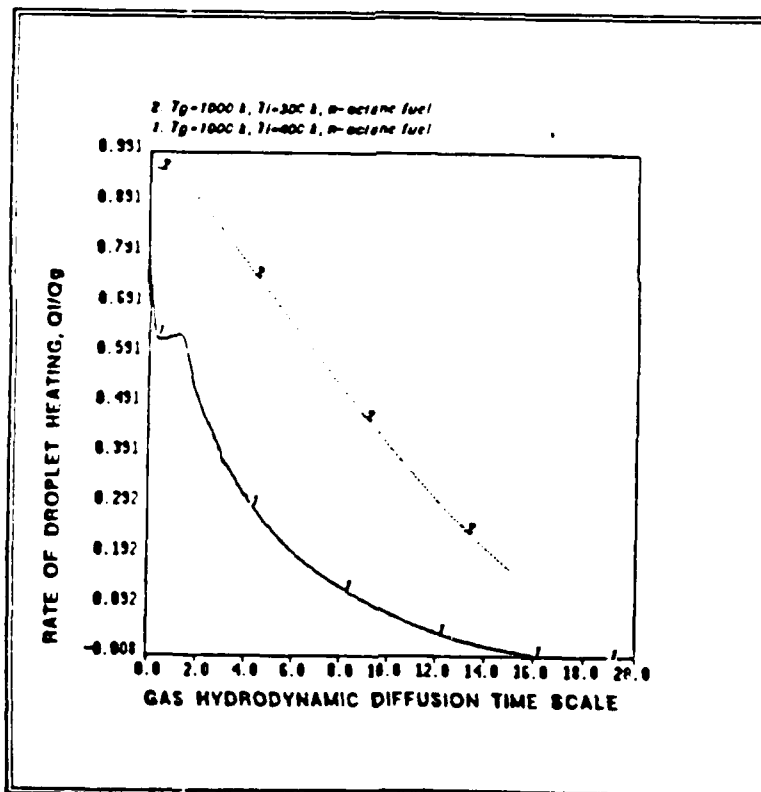
Figure D.5. (a) Time variation of drag coefficients for different initial
droplet temperatures, (b) time variation of the rate of droplet
heating for different initial droplet temperatures.
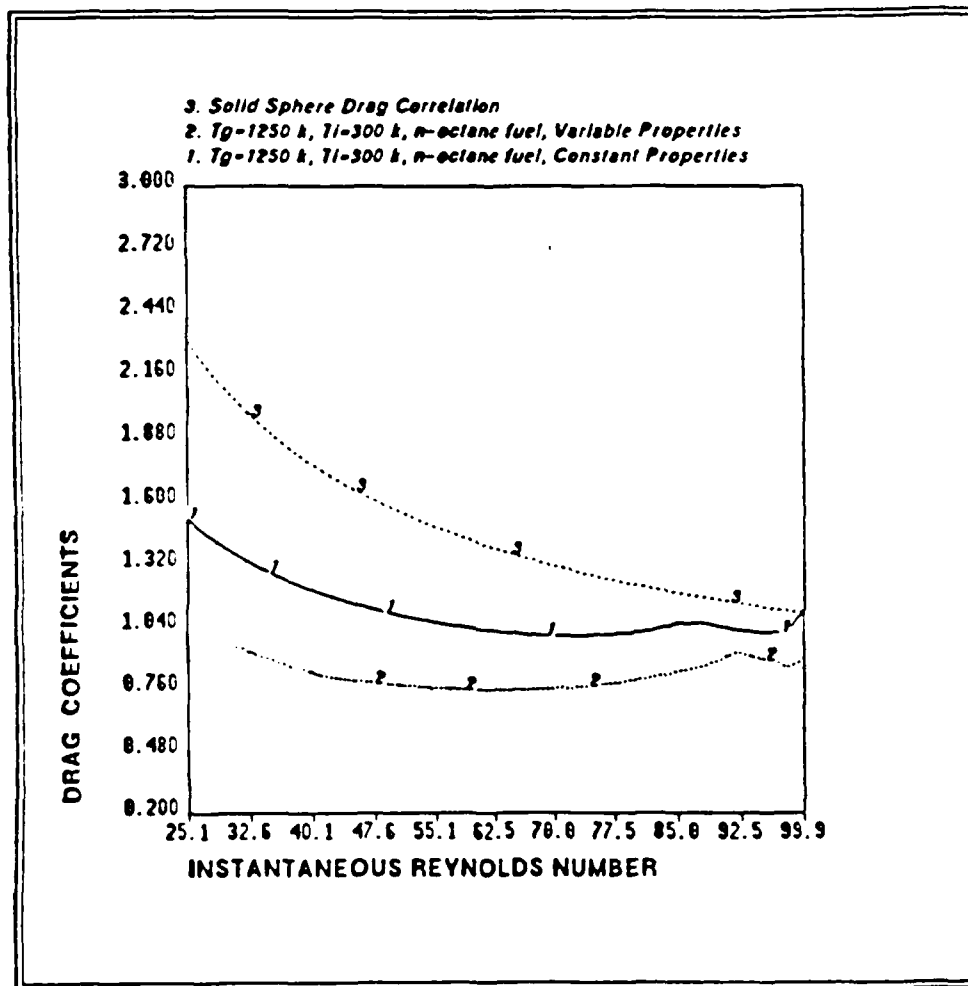
Figure D.6.   Time variation of drag coefficients for constant property case and variable property case.
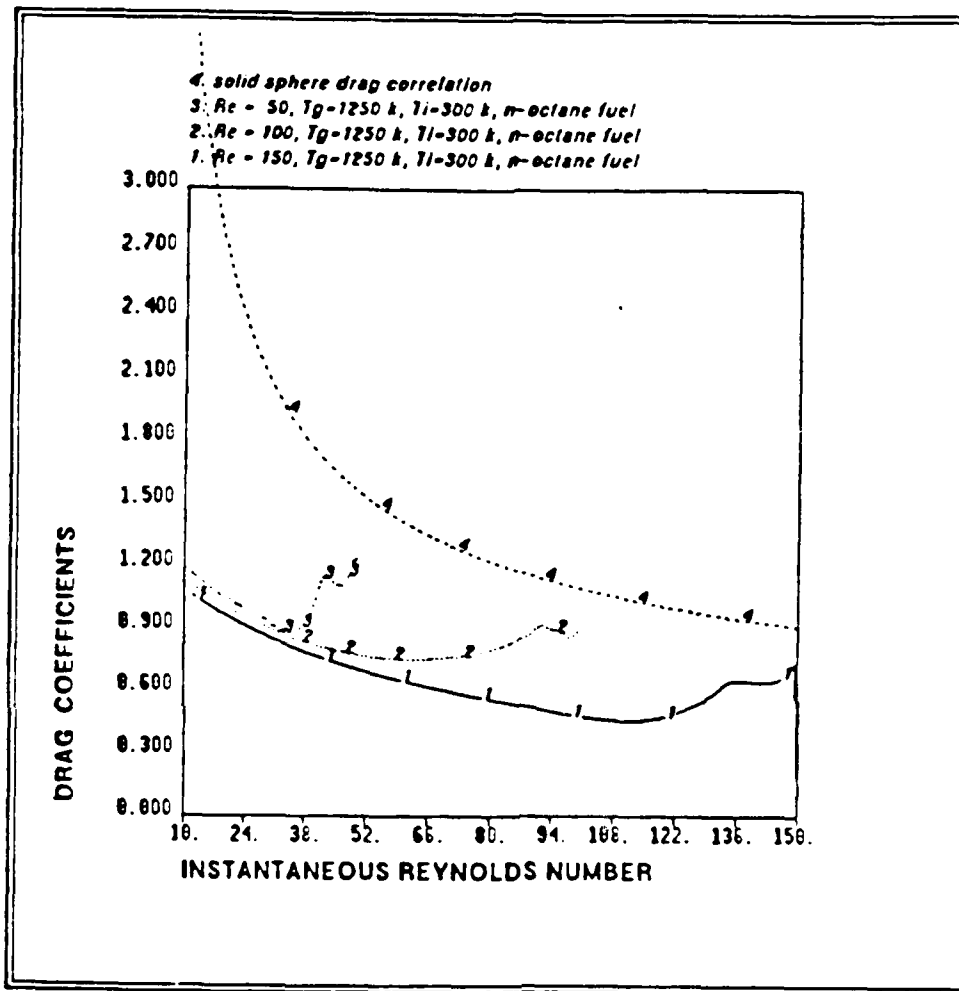
Figure D.7. Time variation of drag coefficients for different initial Reynolds numbers.
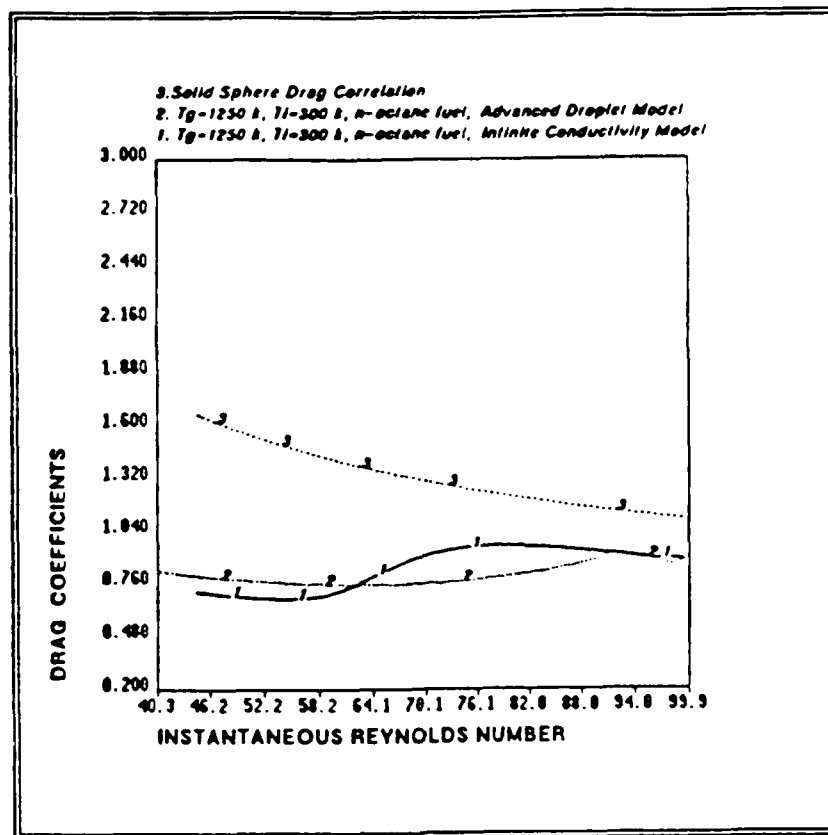
Figure D.8. Time variation of drag coefficients for different droplet heating
models.
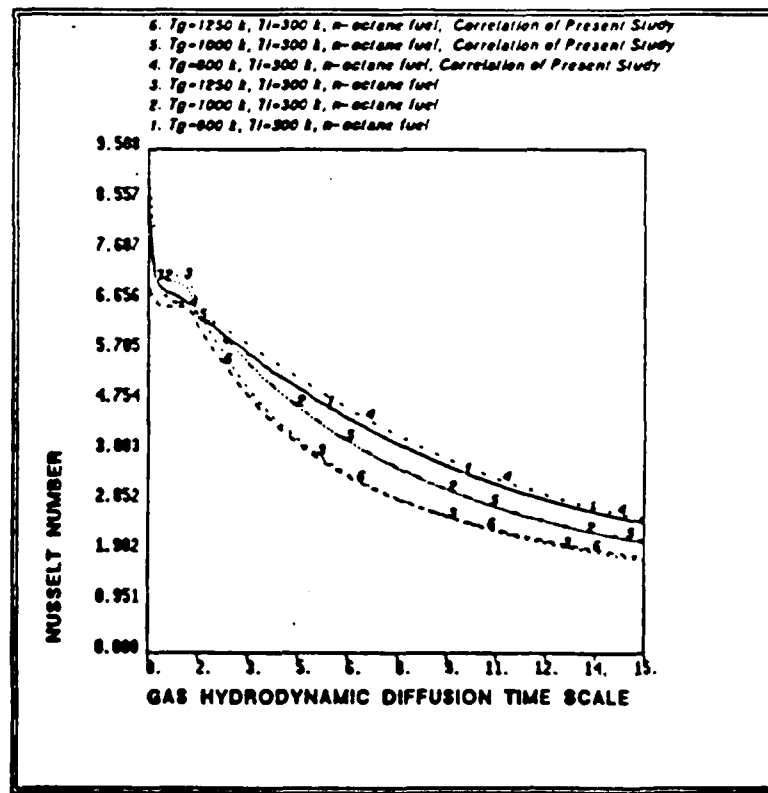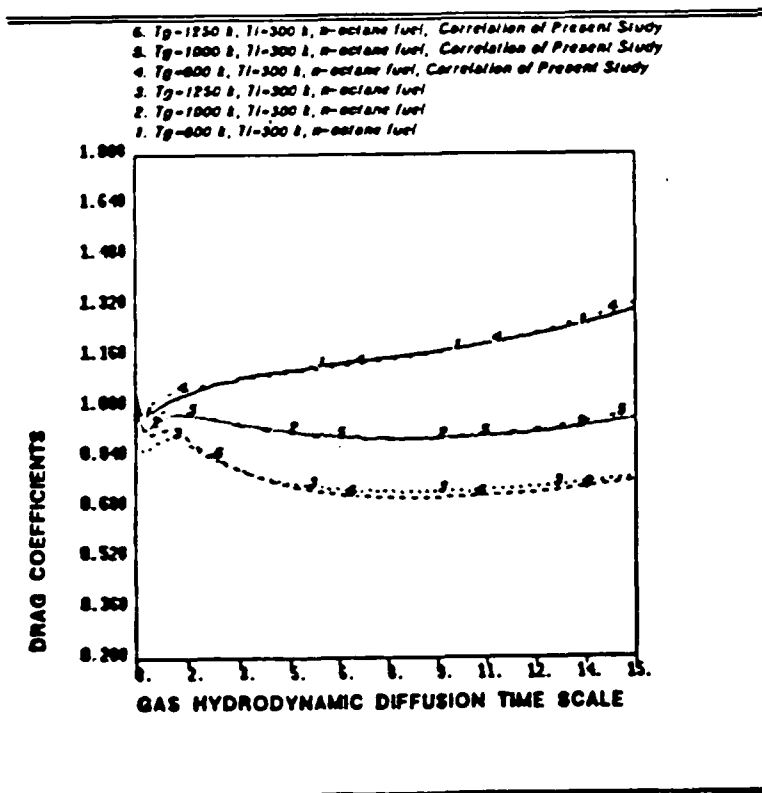
Figure D.9. (a) Comparison of drag coefficients between numerical results and
correlations, (b) comparison of Nusselt numbers between numerical
results and correlations.
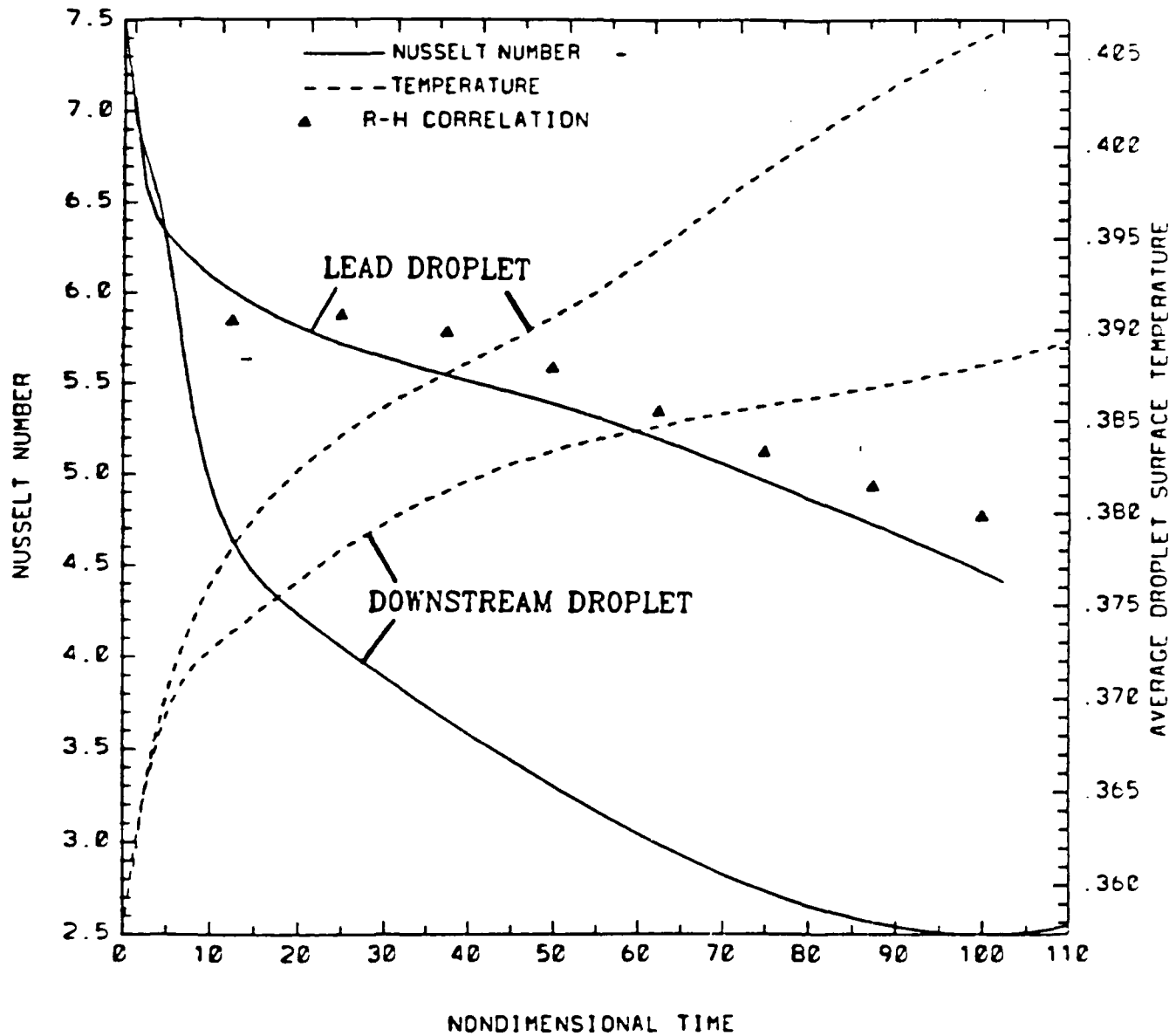
Figure D.10. Time variation of average Nusselt number and droplet surface temperature for approaching droplets.
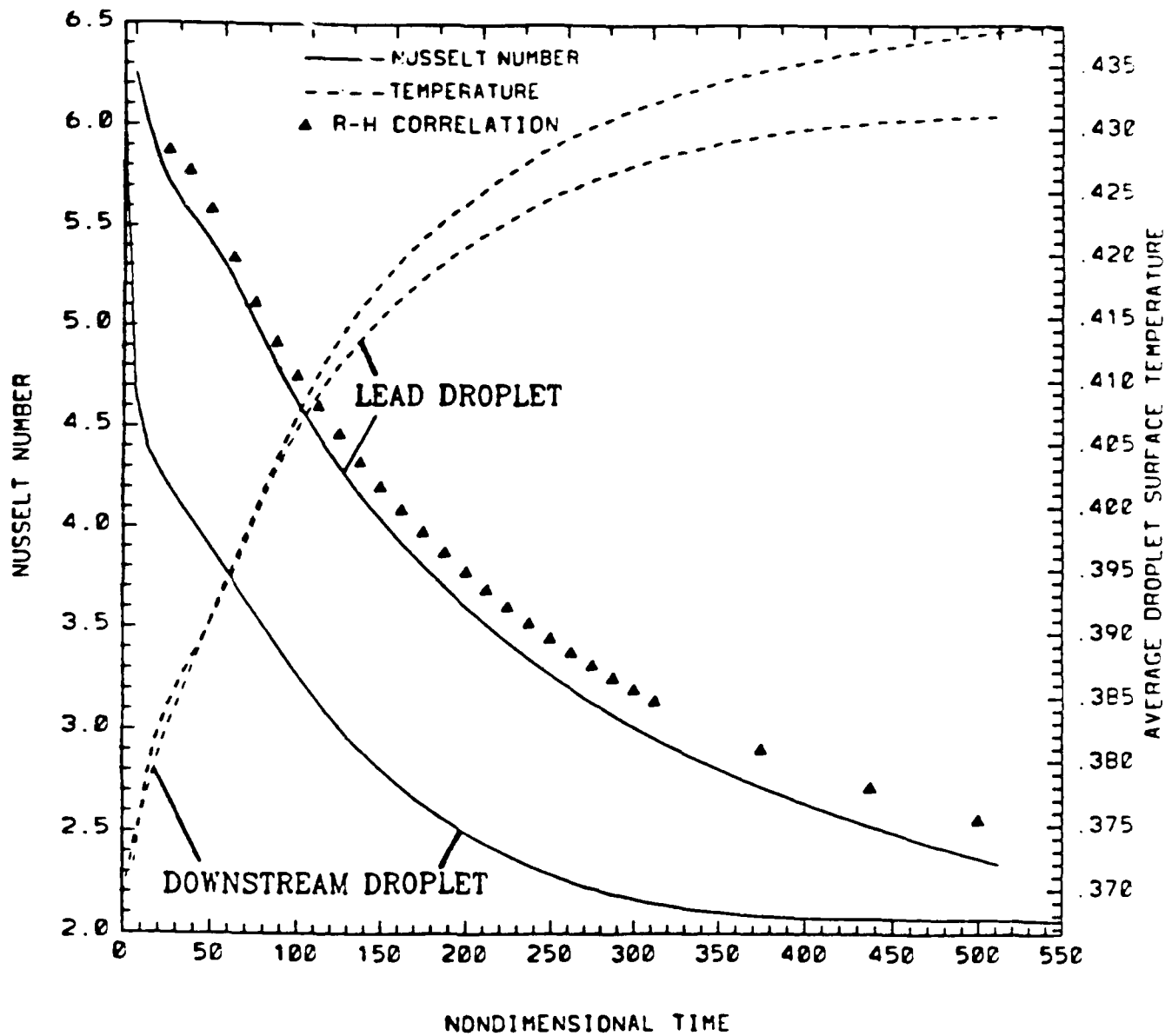
Figure D.11. Time variation of average Nusselt number and droplet surface temperature for separating droplets.